Atmos. Chem. Phys., 13, 2563–2587, 2013
www.atmos-chem-phys.net/13/2563/2013/
doi:10.5194/acp-13-2563-2013

Atmospheric Chemistry and Physics Open Access

Analysis of present day and future OH and methane lifetime in the ACCMIP simulations

A. Voulgarakis[1,2], V. Naik[3], J.-F. Lamarque[4], D. T. Shindell[1], P. J. Young[5,6,7], M. J. Prather[8], O. Wild[7], R. D. Field[9,1], D. Bergmann[10], P. Cameron-Smith[10], I. Cionni[11], W. J. Collins[12,13], S. B. Dalsøren[14], R. M. Doherty[15], V. Eyring[2], G. Faluvegi[1], G. A. Folberth[12], L. W. Horowitz[17], B. Josse[18], I. A. MacKenzie[15], T. Nagashima[19], D. A. Plummer[20], M. Righi[16], S. T. Rumbold[12], D. S. Stevenson[15], S. A. Strode[21], K. Sudo[19], S. Szopa[22], and G. Zeng[23]

[1]NASA Goddard Institute for Space Studies and Columbia Earth Institute, New York, NY, USA
[2]Department of Physics, Imperial College, London, UK
[3]UCAR/NOAA Geophysical Fluid Dynamics Laboratory, Princeton, NJ, USA
[4]National Center for Atmospheric Research (NCAR), Boulder, CO, USA
[5]Cooperative Institute for Research in Environmental Sciences, University of Colorado, Boulder, CO, USA
[6]NOAA Earth System Research Laboratory, Boulder, CO, USA
[7]Lancaster Environment Centre, Lancaster University, Lancaster, UK
[8]University of California at Irvine, CA, USA
[9]Department of Applied Physics and Applied Mathematics, Columbia University, USA
[10]Lawrence Livermore National Laboratory, CA, USA
[11]Agenzia nazionale per le nuove tecnologie, l'energia e lo sviluppo economico sostenibile (ENEA), Bologna, Italy
[12]Met Office Hadley Centre, Exeter, UK
[13]Department of Meteorology, University of Reading, UK
[14]CICERO, Center for International Climate and Environmental Research Oslo, Oslo, Norway
[15]University of Edinburgh, Edinburgh, UK
[16]Deutsches Zentrum für Luft- und Raumfahrt (DLR), Germany
[17]NOAA Geophysical Fluid Dynamics Laboratory, Princeton, NJ, USA
[18]GAME/CNRM, Météo-France, CNRS – Centre National de Recherches Météorologiques, Toulouse, France
[19]National Institute for Environmental Studies, Tsukuba-shi, Ibaraki, Japan
[20]Environment Canada, Victoria, BC, Canada
[21]NASA Goddard Space Flight Center and Universities Space Research Association, Greenbelt, MD, USA
[22]Laboratoire des Sciences du Climat et de l'Environnement, LSCE/CEA/CNRS/UVSQ/IPSL, France
[23]National Institute of Water and Atmospheric Research, Lauder, New Zealand

Correspondence to: A. Voulgarakis (a.voulgarakis@imperial.ac.uk)

Received: 31 July 2012 – Published in Atmos. Chem. Phys. Discuss.: 5 September 2012
Revised: 1 February 2013 – Accepted: 12 February 2013 – Published: 5 March 2013

Abstract. Results from simulations performed for the Atmospheric Chemistry and Climate Modeling Intercomparison Project (ACCMIP) are analysed to examine how OH and methane lifetime may change from present day to the future, under different climate and emissions scenarios. Present day (2000) mean tropospheric chemical lifetime derived from the ACCMIP multi-model mean is 9.8 ± 1.6 yr (9.3 ± 0.9 yr when only including selected models), lower than a recent observationally-based estimate, but with a similar range to previous multi-model estimates. Future model projections are based on the four Representative Concentration Pathways (RCPs), and the results also exhibit a large range. Decreases in global methane lifetime of 4.5 ± 9.1 % are simulated for the scenario with lowest radiative forcing by 2100 (RCP 2.6), while increases of 8.5 ± 10.4 % are simulated for the scenario with highest radiative forcing (RCP 8.5). In this

scenario, the key driver of the evolution of OH and methane lifetime is methane itself, since its concentration more than doubles by 2100 and it consumes much of the OH that exists in the troposphere. Stratospheric ozone recovery, which drives tropospheric OH decreases through photolysis modifications, also plays a partial role. In the other scenarios, where methane changes are less drastic, the interplay between various competing drivers leads to smaller and more diverse OH and methane lifetime responses, which are difficult to attribute. For all scenarios, regional OH changes are even more variable, with the most robust feature being the large decreases over the remote oceans in RCP8.5. Through a regression analysis, we suggest that differences in emissions of non-methane volatile organic compounds and in the simulation of photolysis rates may be the main factors causing the differences in simulated present day OH and methane lifetime. Diversity in predicted changes between present day and future OH was found to be associated more strongly with differences in modelled temperature and stratospheric ozone changes. Finally, through perturbation experiments we calculated an OH feedback factor (F) of 1.24 from present day conditions (1.50 from 2100 RCP8.5 conditions) and a climate feedback on methane lifetime of $0.33 \pm 0.13\,\mathrm{yr\,K^{-1}}$, on average. Models that did not include interactive stratospheric ozone effects on photolysis showed a stronger sensitivity to climate, as they did not account for negative effects of climate-driven stratospheric ozone recovery on tropospheric OH, which would have partly offset the overall OH/methane lifetime response to climate change.

1 Introduction

Oxidation processes remove a range of environmentally important species from the atmosphere. Tropospheric oxidation heavily depends on the levels of the hydroxyl radical (OH) and its geographical distribution (Levy, 1971). Oxidation by OH is the primary loss mechanism for methane (CH_4), the second most important anthropogenic greenhouse gas in the climate system (Forster et al., 2007; Shindell et al., 2009), and an important precursor of tropospheric ozone (O_3) (Logan et al., 1981). Thus, OH abundance and methane lifetime are commonly investigated simultaneously. Besides its role in methane oxidation, OH is also involved in removing trace gases from the atmosphere, through oxidation of atmospheric pollutants such as nitrogen oxides (NO_x), carbon monoxide (CO) and non-methane volatile organic compounds (NMVOCs), and removes ozone-depleting substances such as hydrofluorocarbons (HFCs) from the atmosphere (DeMore et al., 1996). Furthermore, OH participates in the formation of atmospheric aerosols such as sulfate, nitrate and secondary organics (e.g. Koch et al., 2006).

OH production in the atmosphere is initiated by the photolysis of ozone at wavelengths smaller than 330 nm:

$$O_3 + h\nu \rightarrow O_2 + O(^1D)(\lambda < 320\,\mathrm{nm}) \quad \text{(R1)}$$

The product of this temperature-dependent (Atkinson et al., 2004) interaction with sunlight is an excited oxygen atom (O^1D), which can then combine with water vapour to produce two molecules of OH:

$$O(^1D) + H_2O \rightarrow OH + OH \quad \text{(R2)}$$

Thus, high levels of ozone, shortwave radiation and humidity favour the production of OH, and lead to a reduction in the methane lifetime (Logan et al., 1981; Lelieveld et al., 2002). In turn, ozone depends on emissions of its precursors and on climatic conditions; shortwave radiation is modified by overhead absorption by ozone, scattering and absorption by clouds and aerosols, and reflection from the Earth's surface (Madronich, 1987; Voulgarakis et al., 2009a); and water vapour abundances are largely determined by temperature. Since all these factors depend on a variety of physical and chemical processes, understanding of OH on global and regional scales is challenging.

OH has a very short lifetime, on the order of a few seconds (Lelieveld et al., 2004 and reference therein) making measurements particularly challenging. Even with in-situ measurements, its spatial variability makes it difficult to constrain OH abundances at larger spatial scales. For this reason, modelling becomes an essential tool to probe the spatial variability of OH and its drivers, as well as its effects on methane and other species, at different timescales. Globally, the main observational constraint available for the OH abundance and methane lifetime is via methyl chloroform (CH_3CCl_3, also referred to as MCF) measurements (e.g. Prinn et al., 1995; Montzka et al., 2011). Methyl chloroform has fairly well known sources (now almost zero) and very well-known concentrations, which means that the global OH mean concentration can be estimated from the methyl chloroform loss rate.

Past studies have examined the evolution of global OH and methane lifetime since preindustrial times (e.g. Wang and Jacob, 1998; Lelieveld et al., 2002), or their recent trends and interannual variability, using either observations (Bousquet et al., 2005; Manning et al., 2005; Prinn et al., 2005) or models (Dentener et al., 2003; Dalsøren et al., 2006; Fiore et al., 2006). There have also been several model studies examining the potential future evolution of OH and methane lifetime (Thompson, 1992; Lelieveld et al., 1998; Stevenson et al., 2000; Johnson et al., 2001; Prather et al., 2001; Shindell et al., 2006a, b; Stevenson et al., 2006; Wild and Palmer, 2008; Zeng et al., 2010), although the results are not all in agreement. Several of these studies have been performed with chemistry-transport models (CTMs), and often considered only ozone precursor emission effects, without accounting for simultaneous climate changes. Typically, these CTM

studies predicted OH decreases and methane lifetime increases in the future. For example, Lelieveld et al. (1998) found a 6 % increase in methane lifetime from 1992 to 2050 due to increases in CO and methane emissions, both of which consume OH and prolong methane lifetime. However, an earlier study by Thompson (1992) suggested that future changes in OH would most likely be small, due to cancelling effects of methane/CO increases and tropospheric ozone increases. Wild and Palmer (2008), using the SRES A2 emissions scenario (IPCC, 2000), found methane lifetime increases of 13 % in 2100 compared to 2000, with a strong shift in OH abundances from oceanic to tropical continental regions, due to the differing effects of methane and ozone (methane consumes OH while ozone generates it). The model experiments performed in support of the Intergovernmental Panel for Climate Change (IPCC) Third Assessment Report (TAR) fall into this same category of experiments that did not account for climate change effects (Prather et al., 2001). All models calculated global mean OH decreases (and thus methane lifetime increases) between 2000 and 2100, ranging from 6 % to 25 %.

Global modelling studies that took both emissions and climate changes into account were first performed around the time of the publication of IPCC TAR, and, contrary to the studies that only included emission changes, found that future methane lifetime either remained unaffected or significantly decreased. This was attributed to increases in temperature, which drive a faster CH_4+OH reaction as well as higher water vapour concentrations, increasing the rate of the $O^1D + H_2O$ reaction (Stevenson et al., 2000; Johnson et al., 2001). More recently, Zeng et al. (2010) found methane lifetime decreases of 11 % by 2100, using a projection based on the SRES A1B scenario. This supported the earlier findings by Shindell et al. (2006a), whose simulations with a chemistry-climate model (CCM) showed a 10 % decrease in the lifetime, though using the SRES A2 emissions scenario for 2100. Results published around the time of the IPCC Fourth Assessment Report (AR4) projected relatively minor changes in global OH between 2000 and 2030 (Shindell et al., 2006b; Stevenson et al., 2006). Finally, John et al. (2012) found decreasing methane lifetimes between 2000 and 2100 in three out of the four Representative Concentration Pathway (RCP) scenarios used (Meinshausen et al., 2001; van Vuuren et al., 2011), with methane lifetimes increasing only in the extreme RCP8.5 scenario where methane abundances more than double from 2000 to 2100.

Despite the number of studies examining the topic of OH and methane lifetime, there is still no clear consensus on the main issues related to it, not least because there have not been systematic studies focusing on results from multiple composition-climate models, which include many of the processes affecting oxidant changes. Here, we analyse simulations performed for the Atmospheric Chemistry and Climate Modeling Intercomparison Project (ACCMIP, http://www.giss.nasa.gov/projects/accmip/), in support of the IPCC Fifth Assessment Report (AR5), to investigate changes in OH and methane lifetime between 2000 and 2100. This is the first study that uses the RCP scenarios in a multi-model framework to study this topic. ACCMIP includes a variety of CCMs, which were run for the historical period (1850 to present day, with present day defined as year 2000) and for the future (present day to 2100) following the different RCPs. A wide range of chemical output from these simulations is expected to contribute to a deeper understanding of chemistry-climate interactions in long-term climate simulations (e.g. for the Coupled Model Intercomparison Project Phase 5, or CMIP5). This study complements work that is being done under ACCMIP on historical OH and methane lifetime (Naik et al., 2012a), historical and future ozone (Young et al., 2013), and ozone radiative forcing (Stevenson et al., 2012; Bowman et al., 2012; Shindell et al., 2012a). An overview of ACCMIP with an evaluation of present day simulated climate is provided in Lamarque et al. (2013).

In Sect. 2, we will briefly describe the participating models and the simulations performed. Section 3 describes the evolution of OH and methane lifetime between present day and future, while Sect. 4 presents the evolution of potential drivers affecting these quantities. Section 5 analyses model sensitivity experiments that were performed to isolate individual drivers of change, while Sect. 6 describes OH changes on regional scales. Finally, Sect. 7 explores the reasons for model diversity in simulating the quantities of interest and Sect. 8 summarizes the conclusions of the study.

2 Description of models and experiments

2.1 Models

We have used data from 14 models, which performed the future ACCMIP simulations (see Appendix A). Most of the models are CCMs, with the exception of CICERO-OsloCTM2, MOCAGE and STOC-HadAM3. The two former are chemistry-transport models (CTMs), while STOC-HadAM3 produces its own meteorology, but without any interactions with climate. The CCMs were run with an atmosphere-only configuration, with sea-surface temperature and sea-ice data coming either from coupled ocean-atmosphere model simulations or from observations. The models that are linked to coupled climate models that participate in CMIP5 (either because they share the same atmospheric component, or because they use SSTs/SICE generated by CMIP5 models, or both) are: (1) CESM-CAM-superfast (atmosphere-only version of CESM-CAM, using sea surface temperatures (SSTs) and sea-ice (SI) from the latter's CMIP5 simulations), (2) CMAM (based on the preceding generation GCM, but using SSTs/SI from CanESM2 CMIP5 simulations), (3) EMAC (used SSTs/SI from a CMIP5 simulation with the CMCC model, which is, like EMAC, based on ECHAM5, but with differences in the

resolution and shortwave radiation code (Cagnazzo et al., 2007)), (4) GEOSCCM (atmosphere-only version of the GEOS-5 model used for CMIP5, using SSTs/SICE from the CCSM4 model RCP6.0 simulation), (5) GFDL-AM3 (atmosphere-only version of GFDL-CM3, using SSTs/SICE from the latter's CMIP5 simulations), (6) GISS-E2-R (the same runs were used both for CMIP5 and for ACCMIP), (7) HadGEM2 (atmosphere-only version of the model used for CMIP5, but using SSTs/SICE from CMIP3, with the best possible correspondence between RCPs and SRES scenarios), (8) LMDzORINCA (uses SSTs/SI from IPSL-CM4 AR4 simulations), (9) MIROC-CHEM (atmosphere-only version of MIROC-ESM-CHEM, using SSTs/SICE from the latter's CMIP5 simulations), (10) MOCAGE (uses meteorology produced from ARPEGE-Climate atmosphere-only simulations using CNRM-CM5 SSTs/SI from CMIP5 runs), (11) NCAR-CAM3.5 (atmosphere-only version of the model used for CMIP5, but using SSTs/SICE from CMIP3, with the best possible correspondence between RCPs and SRES scenarios), (12) STOC-HadAM3 and 13) UM-CAM (both using SSTs/SI from HadGEM2 coupled CMIP5 simulations). CICERO-OsloCTM2 used ECMWF IFS model forecast data for 2006 for all simulations. Detailed model descriptions are provided in the ACCMIP overview paper of Lamarque et al. (2013). Below we present some of the main features of the models, with an emphasis on those that are important for OH and methane lifetime.

Surface methane concentrations were prescribed in all models (but then methane is allowed to undergo loss processes in the rest of the atmosphere, thus methane burdens will not be exactly identical), except for (a) LMDzORINCA, in which specified emission fluxes were used (see Szopa et al., 2012), and (b) GISS-E2-R, in which interactive emissions for wetlands and prescribed emissions from other sectors were used (see Shindell et al., 2004, 2012b). For prescribing methane concentrations at the surface, most models used data from the database of Meinshausen et al. (2011), except for CICERO-OsloCTM2 and EMAC that used present day methane values from IPCC TAR and from AGAGE (Prinn et al., 2000), respectively, scaled to match the evolution in Meinshausen et al. (2011) in the future. UM-CAM and STOC-HadAM3 are the only models having a globally constant concentration of methane. Note that methane concentrations vary between different time periods in all models.

Anthropogenic and biomass burning emissions of NO_x, CO, and aerosols used in the simulations were identical in all models (Lamarque et al., 2010; 2012a). NMVOC emissions from such sources differ, as the models use a wide range of NMVOC oxidation mechanisms. Also, emissions from natural sources varied widely between the models (Lamarque et al., 2013). The distribution and magnitude of lightning NO_x emissions depend on the model's convection (mostly based on Price and Rind (1992, 1994) and Price et al. (1997); Grewe et al. (2001) was used for EMAC), in all models except GEOSCCM, which used constant global lightning emissions of $5\,Tg\,N\,yr^{-1}$, and CICERO-OsloCTM2 in which the distribution of lightning emissions depends on modelled convection, but with a scaling applied to produce globally constant emissions of $5\,Tg\,N\,yr^{-1}$. Specifically, all models used the cloud top height in order to determine lightning flash rates and hence lightning NO_x emissions, except for CMAM, which used the convective updraft mass flux (Allen and Pickering, 2002). Note that there were some inconsistencies in the implementation of lightning NO_x emissions in HadGEM2 and MIROC-CHEM for this project, which led to those models being outliers in terms of global total lightning NO_x emissions ($1.3\,Tg\,N\,yr^{-1}$ and $9.7\,Tg\,N\,yr^{-1}$, respectively).

Isoprene emissions are climate-sensitive in EMAC, GEOSCCM, GISS-E2-R, and STOC-HadAM3, while the rest of the models use different kinds of estimates, except CMAM and HadGEM2 in which $250\,Tg\,yr^{-1}$ and $475\,Tg\,yr^{-1}$ of CO, respectively, are emitted as proxy for isoprene oxidation. Interactive emissions of other NMVOCs are also included in some models: GISS-E2-R includes climate-sensitive terpene emissions, while in GEOSCCM there are propene and CO emissions as a proxy for terpenes/methanol. EMAC and GEOSCCM include climate-sensitive soil NO_x emissions, while in the rest of the models this source is fixed. Constant fluxes are also assumed for oceanic CO in all models except GEOSCCM and GISS-E2-R. The spread in past, present day and future emissions in the models is shown in Fig. 1 of Young et al. (2013), while more details for the present day spread can be found in Table S1 of Naik et al. (2012a).

Gas-phase chemistry schemes ranged in terms of complexity. The models with more than 100 gaseous species included are EMAC, GEOSCCM, MOCAGE, and NCAR-CAM3.5, while CESM-CAM-superfast had the lowest number of species (16). VOCs other than methane are either not included (CMAM) or included in several different ways in models, with lumping often applied to group NMVOCs in broad categories. Stratospheric ozone in HadGEM2, STOC-HadAM3, and UM-CAM was prescribed following Cionni et al. (2011; in support of CMIP5), while in LMDzORINCA the climatology of Li and Shine (1995) was used. In CICERO-OsloCTM2, monthly model climatological values of ozone and nitrogen species are used, except in the 3 lowermost layers in the stratosphere (approximately 2.5 km) where the tropospheric chemistry scheme is applied to account for photochemical ozone production (Skeie et al., 2011). A simplified scheme was used in CESM-CAM-superfast (McLinden et al., 2000). In the rest of the models, there was a full simulation of stratospheric ozone.

Photolysis treatment in some models broadly follows the approach of using pre-calculated photolysis rates and correcting for real-time atmospheric conditions (clouds, overhead ozone, and, in some cases, surface albedo). On the other hand, CICERO-OsloCTM2, GISS-E2-R, EMAC, GEOSCCM, and MIROC-CHEM used state-of-the-art, fully interactive photolysis schemes (Wild et al. (2000) for the

Table 1. Present day (2000) tropospheric mean (air mass weighted) OH concentration, tropospheric chemical methane lifetime (τ_{OH}), and total methane lifetime (τ) for the 14 participating models. Multi-model means and standard deviations, as well as mean OH concentrations under different tropopause definitions, are also shown. If not indicated otherwise, we integrated the tropospheric OH loss from 200 hPa to the surface. The last row shows the means and standard deviations using a subset of models, excluding HadGEM2 and UM-CAM.

Models	Mean OH (10^5 molec. cm^{-3})	τ_{OH}(chemical) (yr)	τ(total) (yr)[a]
CESM-CAM-superfast	12.9	8.4	7.5
CICERO-OsloCTM2	10.4	10.0	8.7
CMAM	10.8	9.5	8.3
EMAC	11.8	9.2	8.1
GEOSCCM	11.4	9.7	8.5
GFDL-AM3	11.7	9.4	8.3
GISS-E2-R	10.6	10.6	9.2
HadGEM2	8.1	11.4	9.8
LMDzORINCA	10.3	10.4	9.1
MIROC-CHEM	12.5	8.8	7.8
MOCAGE	13.4	7.1	6.4
NCAR-CAM3.5	12.1	9.3	8.5
STOC-HadAM3	12.2	9.0	8.0
UM-CAM	6.5	13.9	11.6
Mean $\pm$ stand. dev.	11.1 ± 1.8	9.8 ± 1.6	8.6 ± 1.2
Mean $\pm$ stand. dev. (with trop1[b])	11.1 ± 1.7	9.7 ± 1.6	–
Mean $\pm$ stand. dev. (with trop2[c])	11.0 ± 1.8	9.8 ± 1.6	–
Mean $\pm$ stand. dev. (selected models)	11.7 ± 1.0	9.3 ± 0.9	8.2 ± 0.8

[a] For the total lifetime, we add to the tropospheric chemical loss a 30 Tg yr^{-1} methane sink in soils and a 40 Tg yr^{-1} sink to the stratosphere (Stevenson et al., 2006).
[b] For trop1, we integrated the tropospheric OH loss from the O_3 = 150 ppb_v surface to the Earth's surface, e.g. Stevenson et al. (2006).
[c] For trop2, we integrated the tropospheric OH loss from the surface defined by 300–215xcos(lat)^2 hPa to the Earth's surface, e.g. Shindell et al. (2006b).

former two; Landgraf and Crutzen (1998) for the latter three), while HadGEM2 and UM-CAM used offline rates (Law and Pyle 1993). These are the only two models where prognostic clouds and overhead ozone column did not affect the photolysis calculations.

For more information on model characteristics, see Lamarque et al. (2013).

2.2 Experiments

The model experiments that are mainly analysed here are the present day and future simulations performed by the ACCMIP models. The models are configured as described in Sect. 2.1. Short-lived precursor emissions (Lamarque et al., 2013) and long-lived species concentrations (Meinshausen et al., 2011) follow the RCPs. There are four RCP emissions/concentrations scenarios, RCP2.6, RCP4.5, RCP6.0 and RCP8.5, with RCP2.6 featuring the least radiative forcing, while RCP8.5 featuring the most. The percentage change in global NO_x, CO and NMVOC emissions between 2000 and 2100 for these scenarios can be seen in Tables 2, S1, S2 and S3. The models were run for different "timeslices", representative of conditions around 2000, 2030 and 2100. In a few cases, simulations were performed for 2010 and 2050 as well. The proposed simulation length for each timeslice was 4–10 yr (after spin-up) using prescribed monthly SSTs (no interannual variations), valid for each timeslice and averaged over 10 yr (see number of simulated years for each model in Lamarque et al., 2013). There are certain gaps in the data provided (e.g. missing variables for some models), but overall the dataset is fairly consistent.

In addition to the above-mentioned simulations, sensitivity experiments were conducted by some modelling teams: a) simulations with present day emissions but climatic conditions set to 2030 or 2100 levels, and b) simulations with perturbed methane concentrations. While these experiments were only performed by a sub-set of the ACCMIP models, in combination with some further tests performed solely with GISS-E2-R they provide further valuable insight into the processes controlling OH and methane lifetime (see Sect. 5.3).

3 Present day and future OH and methane lifetime

3.1 Global changes

Table 1 shows present day (2000) global tropospheric mean OH concentrations, tropospheric chemical methane lifetime

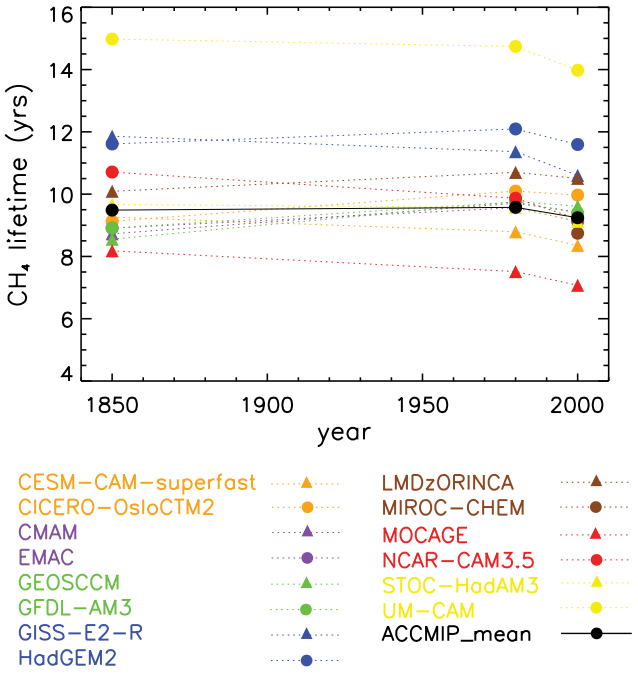

Fig. 1. Evolution of global tropospheric chemical methane lifetime in the ACCMIP models, for the historical period. Multi-model mean values (black dots connected with solid line) were only plotted for timeslices with data from at least 7 models, after removing results from HadGEM2 and UM-CAM.

due to reaction with OH (hereafter referred to as "chemical lifetime"), and total methane lifetime, calculated from all the ACCMIP models. The chemical lifetime is calculated by dividing the global atmospheric methane burden by the global tropospheric chemical loss by OH, while the total lifetime includes the soil and stratospheric sinks in the denominator, following Stevenson et al. (2006). We integrated the tropospheric OH loss from 200 hPa to the surface. No interpolation from the model's native grid has been applied for the calculation of any global quantity. Present day (2000) mean tropospheric chemical lifetime derived from the ACCMIP multi-model mean is 9.8 ± 1.6 yr (9.3 ± 0.9 yr when only including selected models). A recent observation-based analysis (Prather et al., 2012) estimated chemical methane lifetime to be 11.2 ± 1.3 yr, underestimated by most of the ACCMIP models, except CICERO-OsloCTM2, GISS-E2-R, HadGEM2, and LMDzORINCA. Differences between this estimate and the model results is unlikely due to differences in the tropopause used, as Holmes et al. (2013) found that methane oxidation between 200 hPa and the tropopause was less than 1.5 % of total tropospheric oxidation by OH. We also find here that our global tropospheric metrics do not depend on the definition of the tropopause (Table 1), because most OH and methane chemical loss are in the tropical lower troposphere, well away from the tropopause.

A large spread of values for these variables is evident. For example, the simulated chemical methane lifetime ranges from ∼7 yr (MOCAGE) to ∼14 yr (UM-CAM). This spread is of similar magnitude to the ACCENT (Atmospheric Composition Change: the European Network of excellence) studies (Shindell et al., 2006b; Stevenson et al., 2006), conducted around the time of IPCC AR4. The range does not become smaller than in ACCENT even when we select a subset of models following exactly the method of of Stevenson et al. (2006), i.e. all models falling within $\pm 1\sigma$ (not shown). Furthermore, when excluding HadGEM2 and UM-CAM (which are the two models that did not include interactive photolysis) we get a range that is less broad, but not smaller than that calculated using a subset of models in Stevenson et al. (2006). Present day diversity in results will be discussed further in Sect. 7.

Before presenting and analyzing the future evolution of OH and methane lifetime, we briefly discuss the historical evolution of methane lifetime in Fig. 1 (three timeslices). Multi-model mean methane lifetime increases by 2.3 % from 1850 to 1980, however there is large inter-model diversity in the magnitude and sign of change across the models. Of the 14 models included here, six simulate decreases in methane lifetime with the largest reduction simulated by MOCAGE (−8 %) while the rest simulate increases in methane lifetime with the largest increase simulated by GEOSCCM (14 %) over the 1850 to 1980 time period. From 1980 to 2000, all models simulate decreases in methane lifetime with a mean lifetime reduction of 4 %. Evolution of factors driving changes in methane lifetime and OH over the historical period is discussed in further detail in Naik et al. (2012a).

Figure 2 shows the evolution of modelled global chemical methane lifetime between present day and 2100, for the four different RCPs. All the timeslices for which a model performed simulations have been included. The evolution of methane lifetime between different timeslices shows some agreement between different models, in terms of sign. More specifically, in RCP2.6, 7 of the 10 models that provided data show decreases between the beginning and the middle of the 21st century, and a slow increase or stabilization later on. Notable exceptions are the MOCAGE and the NCAR-CAM3.5 models, which mostly show increases throughout the period of study. We note that NCAR-CAM3.5 uses the results from a CCSM3 Commitment simulation as an equivalent for RCP2.6, which leads to an underestimate of the climate effect (see Lamarque et al., 2013) on methane lifetime. The overall change between 2000 and 2100 for RCP2.6 is minimal though (−4.5 % on average). For RCP4.5, for which data from fewer models (7) are available, there is generally a tendency for methane lifetime decreases, especially after 2030. The exception is the GISS-E2-R model, where we find the opposite trend, although with smaller increases than for RCP2.6. Overall, RCP4.5 reveals the largest negative change in global methane lifetime levels relative to 2000 (−8.4 % on average). In RCP6.0 (6 models), there is a mix of positive

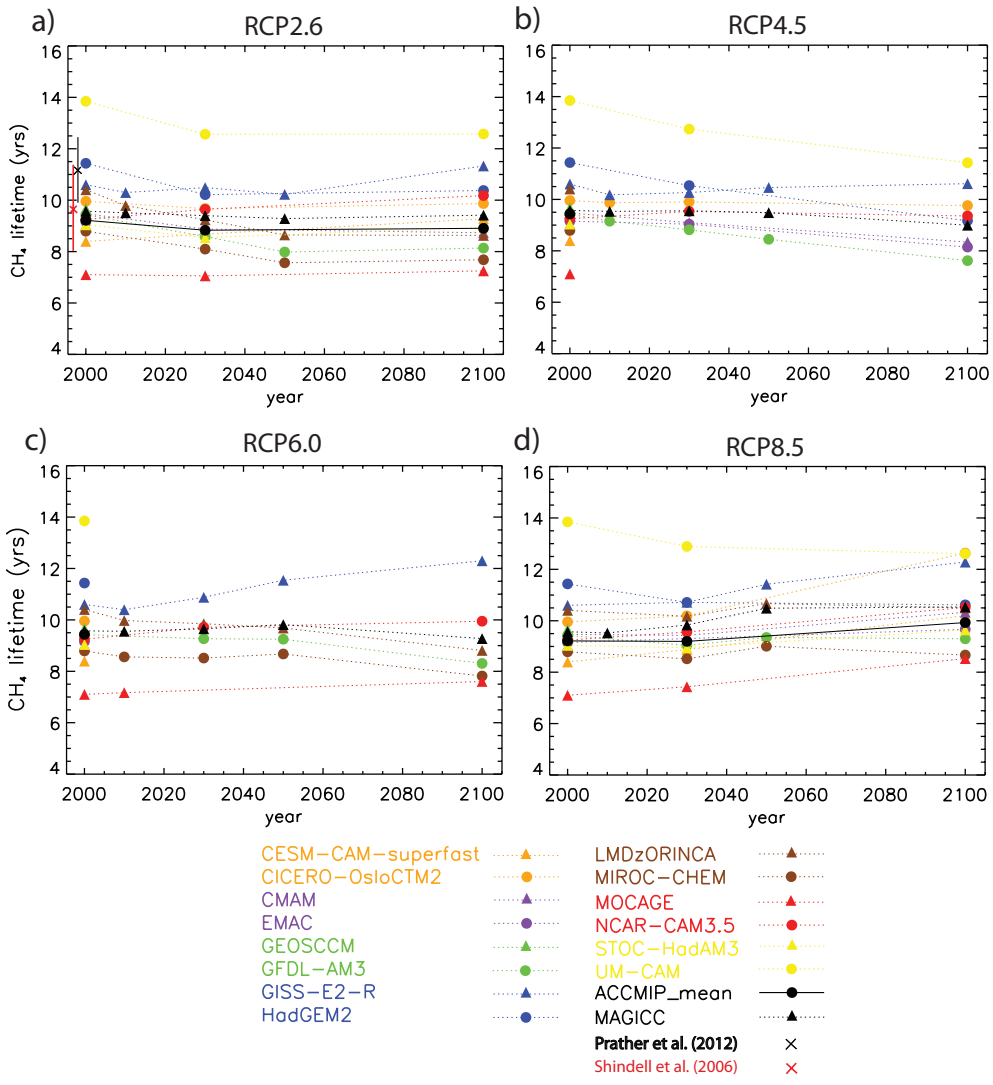

Fig. 2. Evolution of global tropospheric chemical methane lifetime in the ACCMIP models, for the four future RCP scenarios. Multi-model mean values (black dots connected with solid line) were only plotted for timeslices with data from at least 7 models, after removing results from CICERO-OsloCTM2, HadGEM2 and UM-CAM. For comparison, the dotted black line with square points shows the lifetimes used in the MAGICC integrated assessment model. Also, in the upper left panel, the red cross for present day shows the mean chemical lifetime from the ACCENT models (Shindell et al., 2006b), and the black cross is the observationally-based estimate made by Prather et al. (2012).

(2 models) and negative (4 models) trends. Positive trends occur for models that also showed positive trends throughout the RCP2.6 simulation, though in RCP6.0 the changes are more rapid.

The scenario with the highest level of agreement between models, in terms of sign, is RCP8.5 (Fig. S1 also shows the evolution of global tropospheric mean OH and of Northern Hemisphere to Southern Hemisphere OH ratio in this scenario). Nine of the 12 models that simulated this scenario show a methane lifetime increase between 2000 and 2100. From the models that simulated both the 2030 and the 2050 timeslice (5), it is evident that the period with the sharpest increase is 2030-50. This is a period of rapid NO_x emission reductions (not shown; see Lamarque et al., 2013), which could be the driving factor behind the 2030–2050 feature (e.g. see Lelieveld et al., 2002). In general, since OH drives most of the methane loss in the atmosphere, OH changes correspond well to methane lifetime changes seen in the models (see Table 2, and Tables S1, S2 and S3 for other RCPs). The models that have an opposite trend for 2000–2100 are HadGEM2 and UM-CAM. These are also the models with the largest absolute methane lifetimes for present day. Potential reasons for these distinct features will be discussed in Sect. 5.

Table 2. Percentage (%) changes in important model metrics, between 2100 and 2000 (RCP8.5). Variables examined (from left to right) are: global tropospheric air mass-weighted mean OH concentration, global tropospheric chemical methane lifetime, total NO_x emissions (including lightning), total lightning NO_x emissions, total CO emissions, total NMVOC emissions, global atmospheric methane burden, global tropospheric ozone burden, global mean stratospheric ozone column, global volume-weighted tropospheric mean $J(O^1D)$, and global tropospheric mean temperature and humidity. Same tables for the other scenarios are shown in Tables S1, S2 and S3. The last row shows the means and standard deviations using a subset of models, excluding CICERO-OsloCTM2, HadGEM2 and UM-CAM.

Models (RCP8.5)	OH	τ_{OH}	NO_x Emis.	$LiNO_x$ Emis.	CO Emis.	NMVOC Emis.	CH_4 Burd.	O_3 Burd.	Strat. O_3	$J(O^1D)$	T	Q
CESM-CAM-superfast	−17.4	+21.5	−33.0	+29.7	−30.1	0.0	+112.1	+25.1	+5.3	–	0.9	16.1
CICERO-OsloCTM2	−20.6	+26.9	−29.3	0.0	−27.3	−5.8	+108.4	+10.4	+0.3		–	–
CMAM	−15.5	+9.1	−27.2	−45.4	−25.7	–	+114.2	+13.9	+6.4	−4.3	+2.3	+45.3
EMAC	−12.0	+5.6	−22.1	+8.9	−31.5	+17.6	+115.3	+16.2	+6.4	−4.4	+2.2	+37.5
GEOSCCM	–	–	–	–	–	–	–	–	–	–	–	–
GFDL-AM3	−6.7	−1.4	−22.4	+38.2	−30.3	−1.9	+116.1	+27.8	+8.4	−7.2	+2.5	+45.0
GISS-E2-R	−18.6	+15.9	−20.0	+26.2	−35.1	+19.8	+152.7	+27.6	+15.1	−15.0	+1.6	+28.9
HadGEM2	+1.4	−7.11	−25.8	+74.1	−24.0	−22.5	+114.7	+29.0	+10.8	–	+1.9	+35.8
LMDzORINCA	−5.8	+0.9	−31.6	+43.3	−34.7	−4.3	+105.8	+9.6	+0.1	–	+1.9	–
MIROC-CHEM	−6.4	−1.4	−6.9	+38.0	−35.4	−3.4	+116.0	+10.7	+4.2	−0.8	+2.8	+52.2
MOCAGE	−20.1	+20.1	−22.9	+19.9	−32.3	−2.8	+113.4	+28.0	+23.6	–	+1.4	+22.3
NCAR-CAM3.5	−14.1	+13.7	−26.6	+35.2	−30.3	−2.6	+113.9	+14.6	+6.2	−3.6	+1.6	+26.8
STOC-HadAM3	−13.0	+6.7	−20.8	+23.2	−32.4	+25.2	+114.2	+12.1	+5.6	−4.1	+2.3	+38.1
UM-CAM	+2.4	+0.5	−17.2	+43.6	−32.0	−4.2	+112.1	+23.2	+7.4	+0.3	+2.3	+39.0
Mean ± stand. dev.	−11.3 ± 7.7	+8.5 ± 10.4	−23.5 ± 6.8	+24.3 ± 28.7	−30.9 ± 3.5	+1.3 ± 13.2	+116.1 ± 11.4	+19.1 ± 7.7	+7.7 ± 6.2	−4.9 ± 4.7	+2.0 ± 0.5	+35.2 ± 10.8
Mean ± stand. dev. (selected models)	−13.0 ± 5.2	+9.1 ± 8.5	−23.4 ± 7.3	+21.7 ± 25.7	−31.8 ± 2.9	+5.3 ± 11.9	+117.4 ± 12.8	+18.6 ± 7.6	+8.1 ± 6.6	−5.6 ± 4.5	+2.0 ± 0.6	+34.7 ± 11.9

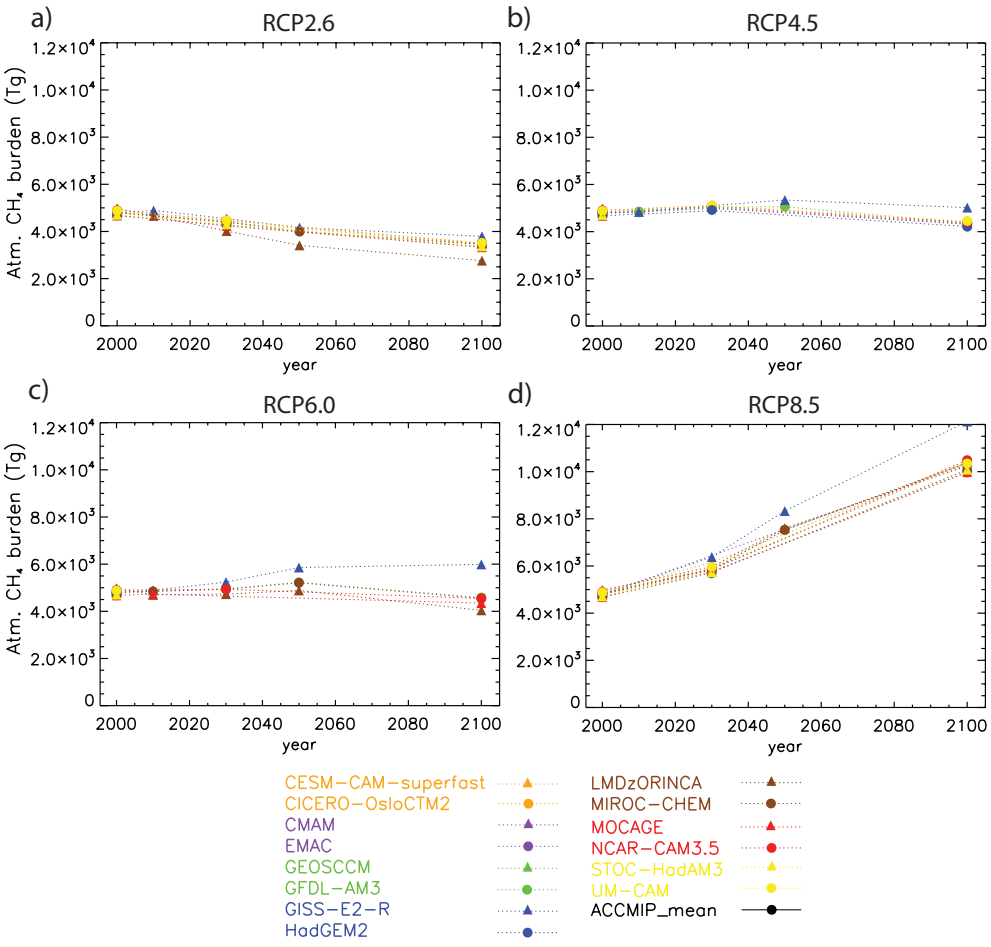

Fig. 3. Evolution of global atmospheric methane burden in the ACCMIP models, for the four different future RCP scenarios. Multi-model mean values (black dots connected with solid line) were only plotted for timeslices with data from at least 8 models.

4 Evolution of potential drivers of OH abundances

Here we provide information on important variables influencing OH and methane lifetime. We consider the evolution of these variables in the 21st century, and especially their 2100 levels. More details on present day emissions and other model metrics are provided by Naik et al. (2012a) and Young et al. (2013).

4.1 Emissions

Global emissions of NO_x decline in all the simulations in the 21st century (Tables 2, S1, S2 and S3; Lamarque et al., 2013). In RCP2.6, RCP4.5 and RCP6.0, the evolution is similar, while in RCP8.5 the trend is less pronounced. Lightning NO_x emissions, which can be a strong driver of OH changes (Labrador et al., 2004; Fiore et al., 2006) are highly uncertain, though they consistently show stronger trends in scenarios with more rapid warming (RPC8.5), since these scenarios often feature greater convective and lightning activity (e.g. Del Genio et al., 2007). A clear exception is CMAM, in which lightning emissions generally decrease with time. This leads to a faster decline of total NO_x emissions in this model compared to the rest. CMAM uses a lightning parameterization based on the convective updraft mass flux from a fixed pressure level (modified version of the method presented in Allen and Pickering, 2002), and the particular trends are due to the changing distribution of the updraft mass flux at that level. The response of the convective updraft mass flux to climate change will likely vary with height and depend on the particular convective parameterization, so trends in lightning NO_x derived from convective mass flux fields will vary with the details of the implementation. Note that, despite the fact that this model is an outlier in terms of lightning NO_x in the current study, decreasing lightning NO_x emissions in a warmer climate were also reported in another study (Jacobson and Streets, 2009).

CO emissions also drastically drop between 2000 and 2100, with RCP2.6 and RCP4.5 showing the most rapid decreases (Lamarque et al., 2013). The good agreement between the trends in different models is due to the fact that

all models used identical anthropogenic and biomass burning emissions, which dominate the totals. Large differences between models within timeslices arise from the fact that some of the models (CMAM, HadGEM2) include proxy emissions (as CO) for NMVOCs. Also, the GISS model does not include oceanic CO sources, which likely explains why it is the model with the lowest total CO emissions. NMVOC emissions have a large spread, but several models show small trends due to static isoprene emissions in all timeslices. In models that include climate-sensitive isoprene emissions (EMAC, GISS-E2-R, STOC-HadAM3), there are detectable positive trends, especially in RCP8.5, which features the largest warming. HadGEM2 NMVOC emissions decrease, but this is only associated with less anthropogenic and biomass burning sources of NMVOCs in 2100, as this model does not include natural hydrocarbon emissions (only proxy CO).

4.2 Methane concentrations

The future evolution of methane burden is shown in Fig. 3, while 2000-2100 changes can be seen in Tables 2, S1, S2 and S3. As mentioned above, methane concentrations are imposed in the models and there are no sources included, with the exception of the LMDzORINCA (past/future) and the GISS-E2-R model (future). There are clear differences between the resulting methane burdens in the different timeslices. In RCP2.6, methane decreases steadily throughout the century, in RCP4.5 it remains steady until 2050 and then decreases, in RCP6.0 it increases until 2050 and then decreases, and in RCP8.5 it rapidly increases throughout the century and is double in 2100 compared to 2000. Most models agree fairly well in the methane burden, with the exception of the GISS-E2-R model which, especially in RCP8.5, shows a faster methane increase and significantly higher burden by the end of the century. This is due to the fact that in future GISS-E2-R simulations (in which surface methane emissions rather than concentrations are prescribed), changes in methane emissions affect OH concentration, and thus feedback to methane's own lifetime (see Fig. 2), which means that methane increases amplify themselves during the 21st century. For more discussion on GISS-E2-R methane behavior, see Shindell et al. (2012b).

4.3 Meteorological factors

The most important meteorological factor affecting OH and methane lifetime is tropospheric humidity (Spivakovsky et al., 2000). Higher water vapour concentrations in the troposphere, mean that more OH is produced through reaction with singlet oxygen atoms (O^1D). Temperature can be directly and indirectly linked to OH and methane lifetime by (a) affecting the CH_4+OH reaction rate and the absorption cross section of ozone (which is important for photolysis to produce O^1D), and (b) through its positive effect on tropospheric humidity. There are several other direct and indirect ways in which temperature and humidity can impact OH and methane lifetime (through effects on other chemicals, aerosols, and feedbacks into the circulation), but they are generally expected to be smaller than those described above.

Clouds, which impact photolysis, and thus affect OH levels, should have relatively small effects on a global scale (e.g. Voulgarakis et al., 2009b), and more significant effects on regional scales. However, since we do not currently have cloud data from a sufficient number of ACCMIP models, we intend to examine this driver of OH variability further in a future study. The same is true for surface albedo, another factor that can strongly affect regional OH (Voulgarakis et al., 2009c)

Apart from CICERO-OsloCTM2, which used fixed meteorological fields for every simulation, global mean temperature changes are positive in all scenarios (Tables 2, S1, S2 and S3), due to the increases in greenhouse gas concentrations. The smallest temperature changes (+1.3 K on average) are found in RCP2.6 and the largest ones (+4.6K on average) in RCP8.5. There is a sizeable spread in the modelled temperature changes projected for 2100 (e.g $\pm 90\,\%$ spread around the mean change for RCP8.5). This is particularly important, as temperature can be rather effective in driving OH and methane lifetime changes (Wild, 2007). There is a strong relationship between the CH_4 + OH reaction rate constant (k) and temperature (see Appendix A), which implies that small changes in temperature can drive relatively large changes in methane loss.

Regarding humidity, the main features of change are similar to those of temperature, but with larger relative differences between timeslices. The models with the highest global mean temperature also have the highest global mean humidity (also see Naik et al., 2012a). For more details on ACCMIP simulated climate, see Lamarque et al. (2013).

4.4 Ozone and ozone photolysis

Tropospheric ozone can affect OH and methane lifetime directly due to the fact that its photolysis provides the O^1D atoms that react with water vapour to produce OH. Thus, increases in ozone precursors can increase the OH levels in the troposphere. Stratospheric ozone affects tropospheric OH indirectly. First of all, changes of the amounts of stratospheric ozone entering the troposphere will affect the levels of tropospheric ozone available for OH production. Perhaps more importantly, stratospheric ozone changes affect shortwave radiation reaching the troposphere to drive photolysis.

Tropospheric ozone changes in the ACCMIP simulations are shown in Tables 2, S1, S2 and S3, and documented thoroughly by Young et al. (2013). Briefly, tropospheric ozone burden declines throughout the 21st century ($-14.1 \pm 6.5\,\%$ in 2100, using all models) in RCP2.6, due to decreasing precursor emissions and decreasing methane concentrations. RCP4.5 and RCP6.0 have minor differences between 2000 and 2100, while RCP8.5 features large increases

($+19.1 \pm 7.7$ %), due to the impact of the dramatic methane increases and possibly due to enhanced stratospheric influx (see also Kawase et al. 2011; Young et al. 2013).

All the scenarios show a recovery of stratospheric ozone abundances in the future, as they all take into account the measures for continued controlling emissions of ozone depleting substances. This recovery is faster in RCP8.5, due to CO_2-induced cooling of the stratosphere and enhanced circulation leading to a faster recovery of stratospheric ozone in this scenario (e.g. Eyring et al., 2010). Of the models that simulate stratospheric ozone, those with the fastest ozone recovery are GISS-E2-R, HadGEM2 and MOCAGE. LMDzORINCA shows no stratospheric ozone changes, due to the fact that an offline ozone climatology was used (Li and Shine, 1995).

Data for photolysis rates of ozone to yield O^1D (JO^1D) were only provided by a fraction of the models. In most cases there is a detectable decrease in $J(O^1D)$, and it relates to the increase of overhead ozone. However, only one model (GISS-E2-R) shows global $J(O^1D)$ decreases that are sizeable (6–15 %) in all RCPs. The GISS-E2-R results on stratospheric ozone and $J(O^1D)$ may partly be an overestimate, as this model has been found to have an ozone hole that extends slightly too far equatorward in September-October and persists about one month too long in the polar region (Shindell et al., 2012b). Note though, that the other two models in which we found more rapid stratospheric ozone recovery did not include ozone changes in photolysis calculations (HadGEM2) or did not provide $J(O^1D)$ data (MOCAGE).

5 Discussion on the drivers of OH and methane lifetime changes

5.1 Emissions

Generally, increases in NO_x emissions have been associated with more OH generation, for two reasons: (a) NO_x generally leads to ozone production (except under high NO_x conditions typically not represented in global models), which is the main primary source of OH, and (b) NO_x-rich environments favour more efficient secondary OH production through HO_x recycling processes (e.g. conversion of HO_2 to OH) and, thus, increase OH abundances in the troposphere (e.g. Lelieveld et al., 2002). However, despite the fact that global NO_x emissions decrease substantially in all scenarios and models between 2000 and 2100, the trends in global mean OH and methane lifetime have diverse signs in different models in RCP2.6, RCP4.5 and RCP6.0 (Fig. 2). Furthermore, these trends are rather small, supporting the idea that global OH may be a relatively stable quantity, despite the large fluctuations on regional scales (Lelieveld et al., 2002). RCP8.5 is the only scenario in which NO_x emissions and global OH are related in terms of sign of change (both decreasing). However, we will demonstrate in Sect. 5.2 that NO_x changes are not the main driver of the global OH trends.

Emissions of CO, which consumes OH, also generally drop during the 21st century. We speculate that they most likely do not play a central role in driving OH and methane lifetime changes, since (a) the latter show fairly diverse trends in RCP2.6, RCP4.5 and RCP6.0, despite the large CO emissions decreases, and (b) in RCP8.5, global mean OH decreases, which could have been explained by increasing CO emissions, while CO emissions decrease in this scenario. Emissions of NMVOCs change significantly only in GISS-E2-R, EMAC and STOC-HadAM3 (and most prominently in RCP8.5), since these are the only models that include climate-sensitive isoprene emission. However, these relatively small increases cannot be the main driver of the sizeable OH and methane lifetime changes, which are found in most models in RCP8.5 (See Fig. 2).

Methane burden changes (Fig. 3) do not appear to be the main driver of the evolution of OH and methane lifetime for RCP2.6. In the latter part of the 21st century the methane burden slowly decreases, which would drive less OH consumption; however, OH and methane lifetime remain fairly unaffected. In RCP8.5, it is likely that methane changes are a major driver of OH and methane lifetime changes, something that is examined in more detail in Sect. 5.2.

5.2 Sensitivity experiments

We have performed a variety of sensitivity experiments based on RCP8.5, and a few based on RCP6.0, in order to understand the methane lifetime trends in these simulations (see Table 3). RCP8.5 has been selected as the focus, as it is a scenario with a somewhat better agreement between models in terms of the sign of the changes, with an increase in methane lifetime in most of the models.

Some of the sensitivity simulations were specifically requested by ACCMIP, and were performed by more than one model. This includes (a) a simulation with ozone precursor emissions set to 2000 values, but with climate set to 2100 RCP8.5 conditions (Cl2100); (b) a simulation with present day conditions but methane concentrations increased by 100 ppb, with this perturbation affecting the modelled chemistry only (CH42000+100); and (c) a simulation with 2100 RCP8.5 conditions, but with methane concentrations perturbed by 100 ppb. In addition, we performed some extra simulations with the GISS-E2-R model, in order to examine some other potential driving factors: (d) ODS2100, in which we used present day conditions, but set ozone depleting substance (ODS, namely chlorofluorocarbons (CFCs) and nitrous oxide (N_2O)) to 2100 levels following the projections in RCP8.5, (e) CH42100a, in which we used present day conditions but methane concentrations corresponding to 2100 RCP8.5 levels, and (f) CH42100b, in which we used present day conditions but methane concentrations corresponding to 2100 RCP6.0 levels.

Table 3. List of sensitivity experiments.

	Cl2100	ODS2100	CH42000 + 100	CH42100a	CH42100 + 100	CH42100b
SSTs/SICE	2100 RCP8.5	2000	2000	2000	2100 RCP8.5	2000
CO_2	2100 RCP8.5	2000	2000	2000	2100 RCP8.5	2000
CH_4	2000*	2000	2000+100 ppb	2100 RCP8.5	2100 RCP8.5+100 ppb	2100 RCP6.0
CFCs/N_2O	2000*	2100 RCP8.5	2000	2000	2100 RCP8.5	2000
NO_x/CO/NMVOCs	2000*	2000	2000	2000	2100 RCP8.5	2000

* Only for chemistry. For climate it follows the rest of the simulation.

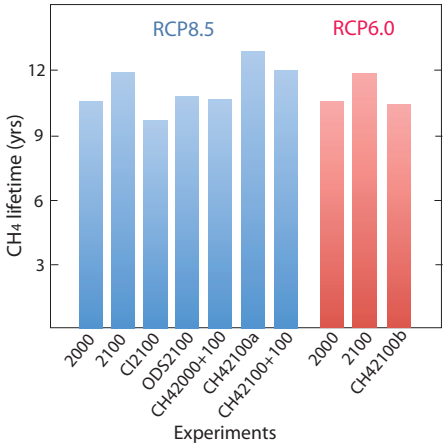

Fig. 4. Tropospheric chemical methane lifetime in the sensitivity experiments performed with the GISS-E2-R model.

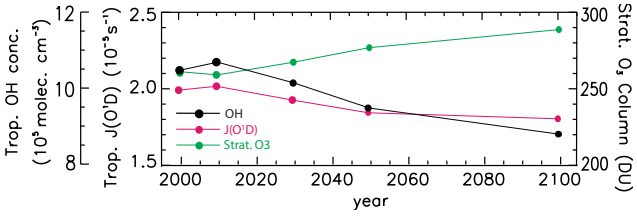

Fig. 5. Global tropospheric air mass-weighted OH concentration, volume-weighted tropospheric mean $J(O^1D)$ and stratospheric mean ozone column (above 200hPa) in the RCP6.0 simulation from the GISS-E2-R model.

By comparing results for 2000 and Cl2100 (Fig. 4 and Table 4), we find that climate changes lead to methane lifetime decreases in the future, in agreement with previous studies (e.g. Stevenson et al., 2006). Warmer temperatures and higher humidity levels drive increases in atmospheric OH and faster CH_4+OH reaction, thus resulting in a shorter lifetime. Furthermore, drastic increases in STE in a warmer climate (Kawase et al., 2011; Young et al., 2013) lead to more ozone and, thus, more OH in the troposphere. However, the 2100 simulation shows increases in methane lifetime during the 21st century. Thus, climate alone would have opposite effects to those found in our future simulations, in which the climate effects have probably only contributed to offsetting some of the positive changes (by ∼1.6 yr, in 2100 for RCP8.5; see Table 4). By comparing 2000, 2100 and ODS2100, it is evident that ODSs have a sizeable effect on methane lifetime. However, this is not enough to explain the changes between 2000 and 2100. We conclude it is methane abundance itself that actually drives the largest part of the 2000–2100 changes in RCP8.5: in the CH42100a simulation, methane lifetime exceeds the levels of 2100. The consumption of OH radicals by increasing methane abundances leads to a drastic decrease of methane loss rates, and thus a prolonged lifetime. The further increase above the 2100 levels would have most likely been offset had there been climate changes included in the simulation.

However, for RCP6.0 (red bars in Fig. 4), we find that methane burden changes cannot explain the 2000-2100 increases in methane lifetime. Despite substantial increase in RCP6.0 methane concentrations in the GISS model (see Fig. 3), the results from CH42100b are almost identical to the 2000 simulation. Thus, when methane changes are not as dramatic as in RCP8.5, the influence of other factors becomes more prominent. In this case, a combination of NO_x emission decline and stratospheric ozone recovery leading to lower $J(O_1D)$ are the most likely drivers. Particularly $J(O^1D)$ shows a strong correlation with both the stratospheric ozone column and with tropospheric OH throughout the 21st century (Fig. 5).

5.3 Climate penalty and OH feedback factors

The Cl2100 simulation, as well as a similar one (Cl2030) with climatic conditions set to 2030 (Cl2030), were performed by several ACCMIP models. Such simulations are useful in order to determine the "climate penalty factor" (defined in earlier studies as the relationship between ozone and temperature; e.g. Wu et al., 2009) for methane lifetime, i.e. the lifetime perturbation by a unit change of global temperature. We get a multi-model mean value of $-0.31 \pm 0.14\,\mathrm{yr\,K^{-1}}$ from the Cl2030 simulation and $-0.34 \pm 0.12\,\mathrm{yr\,K^{-1}}$ from Cl2100 (Table 4). For most models, the estimate from the different timeslices is similar, though in the GISS-E2-R model the differences are more substantial. The models with the strongest methane lifetime

Table 4. Global tropospheric chemical methane lifetime change in the climate change sensitivity simulations, and lifetime change per unit change of global temperature (or "climate penalty factor"), for the different ACCMIP models. The multi-model mean and standard deviation are also shown. The last row shows the means and standard deviations using a subset of models, excluding HadGEM2 and UM-CAM.

	$\Delta\tau_{OH}$ (yr) Cl2030–2000	$\Delta\tau_{OH}$ (yr) Cl2100–2000	$\Delta\tau_{OH}/\Delta T$ (yr K^{-1}) Cl2030–2000	$\Delta\tau_{OH}/\Delta T$ (yr K^{-1}) Cl2100–2000
CESM-CAM-superfast	−0.30	−0.72	−0.29	−0.32
CICERO-OsloCTM2	–	–	–	–
CMAM	–	–	–	–
EMAC	–	–	–	–
GEOSCCM	–	–	–	–
GFDL-AM3	−0.54	−1.82	−0.32	−0.29
GISS-E2-R	−0.08	−0.88	−0.12	−0.22
HadGEM2	–	−2.40	–	−0.50
LMDzORINCA	–	–	–	–
MIROC-CHEM	−0.59	−2.08	−0.36	−0.30
MOCAGE	−0.09	−0.86	−0.21	−0.25
NCAR-CAM3.5	−0.34	−1.48	−0.40	−0.40
STOC-HadAM3	−0.31	−1.21	−0.22	−0.21
UM-CAM	−0.81	−3.08	−0.57	−0.54
Mean ± stand. dev.	-0.38 ± 0.25	-1.61 ± 0.80	-0.31 ± 0.14	-0.34 ± 0.12
Mean ± stand. dev. (selected models)	-0.32 ± 0.20	-1.29 ± 0.52	-0.27 ± 0.10	-0.28 ± 0.07

response and the strongest response per unit temperature change are HadGEM2 and UM-CAM. This may be explained by the fact that those two models are the only ones that do not include the effect of modelled overhead ozone column on photolysis, which would have driven an offsetting of the negative climate effect on methane lifetime, since stratospheric ozone is expected to increase in a warmer climate (Eyring et al., 2010). Note that HadGEM2 and UM-CAM are also the models with the highest present day methane lifetimes (Table 1), however even in relative terms these models are among the three with the strongest methane lifetime response in the Em2000Cl2100 simulation.

In addition to the above sensitivities, two models also performed runs in which methane concentrations were perturbed by a small amount (100 ppb_v), in order to detect the sensitivity of oxidants and methane lifetime to changing methane abundances. 2000CH4plus100 is a simulation identical to baseline 2000, but with methane increased by 100 ppbv, while 2100CH4plus100 is the equivalent for 2100 RCP8.5 conditions. The "feedback factor (F)" (Table 5) is defined as the ratio of the atmospheric response time (timescale of a perturbation) to the global atmospheric lifetime,

$$F = 1/(1 - s) \quad (1)$$

where

$$s = (\delta \ln(\tau))/(\delta \ln[CH_4]) \quad (2)$$

using values for the methane lifetime (τ) and concentration [CH_4] determined from the simulations (as per Fiore et al., 2009; Prather et al., 2001). In Table 5, we also provide $\delta\ln(\tau_{OH}))/(\delta\ln\,[CH_4])$ which is often used in a similar context.

The F values that we get from the four simulations range from 1.19 to 1.53 (Table 5). The values obtained from the 2000CH4plus100 simulation are somewhat closer than those obtained from 2100CH4plus100 to the estimates of Fiore et al. (2009), which were also based on perturbed present day conditions. However, note that our results are only based on two models, and that our present day estimates, though closer to Fiore et al. (2009), are still significantly lower than in their study. The differences between the present day and the future perturbation simulations in our study are larger than the differences between the two models' estimates for the same perturbation. An atmosphere with very high abundances of methane and very low abundances of NO_x, such as in the RCP8.5 scenario, would feature less OH recycling (Lelieveld et al., 2002), and so a stronger effect of methane on its own lifetime. Note that in Prather et al. (2001), F did not change drastically when evaluated in a high methane (4300 ppb; see their Table 4.3) atmosphere. However, in that case, NO_x emissions followed the A2 scenario, and F was not evaluated under low NO_x conditions, as done here.

6 Regional OH changes

While global tropospheric OH is important in determining the lifetimes of various climate-relevant species, it is also crucial to understand the distribution and evolution of OH in the boundary layer, as it reflects the characteristics of the local photochemistry in different areas. A detailed analysis

Table 5. Feedback factor (F)* and related quantities from two of the ACCMIP models and two different simulations (one for present day conditions (2000) and one for future (2100)). τ refers to the global total methane lifetime and τ_{OH} for the global tropospheric chemical lifetime.

Experiment	$\Delta \ln(\tau)/\Delta \ln(CH_4)$	$\Delta \ln(\tau_{OH})/\Delta \ln(CH_4)$	F
2000CH4plus100 GISS-E2-R	0.16	0.19	1.19
2100CH4plus100 GISS-E2-R	0.35	0.41	1.53
2000CH4plus100 UM-CAM	0.22	0.26	1.28
2100CH4plus100 UM-CAM	0.32	0.38	1.46

* F is used in order to calculate the perturbation lifetime, $\tau_{pert} = \tau F$. This perturbation lifetime accurately describes the lifetime of a perturbation in the current atmosphere, For methane and other well-mixed greenhouse gases, the decay of a perturbation is closely approximated by an e-fold time of τ_{pert}.

of the regional features of OH and its future changes in different models would require investigation of the distribution of emissions and of each model's regional climate response. Such a detailed analysis is not within the scope of the current study, which mainly aims to discuss the evolution of OH and methane lifetime on a global scale. However, below we present the main features of the regional behavior of OH, and we aim for further regional analysis in a future study.

Figure 6 shows the multi-model mean change in surface (model level 1) OH concentration between 2100 and 2000 for RCP2.6 and RCP8.5 (the equivalent plots for individual models are shown in Figs. S2 and S3). We focus on those two simulations because they represent the extreme cases from a climate point of view. In RCP2.6, the model mean shows a mixture of positive and negative changes in the Southern Hemisphere. Negative differences are largely found in the Northern Hemisphere, especially in RCP2.6, attributable to the methane increases and to reductions in NO_x emissions. There are notable strong OH increases in both scenarios over western Europe. These may be associated with a more dominant role of CO reductions, which drive OH increases, rather than NO_x effects. However, note that this effect is not seen in all models (Figs. S2 and S3). For example, in HadGEM2, positive changes over Europe are dramatic, whereas in GISS-E2-R there are solely negative changes. Another prominent feature is the reduction along ship tracks in RCP2.6, due to the reduction in shipping NO_x emissions in this scenario (Fig 6b). Overall, there is a rough tendency for a redistribution of OH from the northern midlatitudes to the tropics, as was also discussed in previous studies (e.g., Gupta et al., 1998; Wild and Palmer, 2008).

OH abundance mostly decreases in the Southern Hemisphere in the RCP8.5 with decreases up to 50 % in the Southern Ocean. Over the oceans, despite the increases of water vapour in RCP8.5, the dominant factor driving OH changes most likely is methane, since it has a long-enough lifetime to travel away from its source regions and be relatively well-mixed in the troposphere. This is consistent with the ubiquitous OH reductions in RCP8.5 (which is a scenario that features very large methane increases) over oceanic regions, in qualitative agreement with Wild and Palmer (2008). Negative

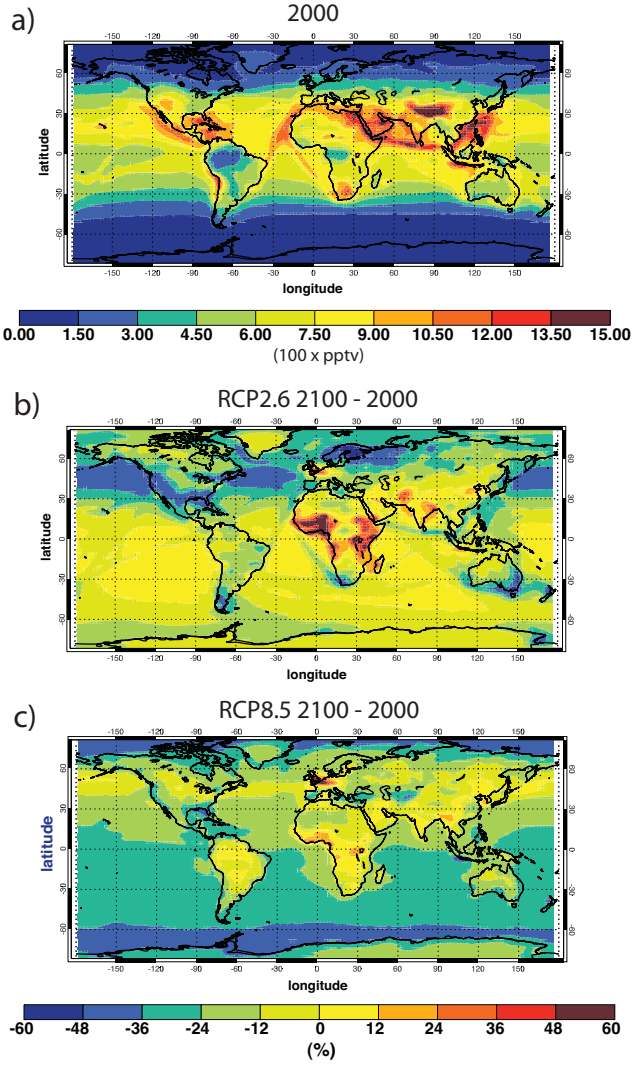

Fig. 6. Multi-model mean surface annual mean OH concentration for present day **(a)**, and its change between 2000 and 2100 in RCP2.6 **(b)** and RCP8.5 **(c)**. The bottom model layer results have been used as representative for the surface. Please see Figs. S2 and S3 for surface OH changes in individual models.

changes are even larger at high southern latitudes (Fig. 6c), possibly due to the additional effect of stratospheric ozone depletion: ozone recovery leads to less radiation reaching the troposphere, slower photolysis and, thus, less OH being produced. Models that do not include the effects of simulated ozone in photolysis calculations (HadGEM2, UM-CAM), do not have this high-latitude feature.

The agreement with Wild and Palmer (2008) is not as evident over land as it is over oceans. Their work, which was based on the SRES A2 scenario, found OH increases over all continental areas in 2100. In our case features are more mixed, with parts of continental areas actually experiencing negative OH changes, most likely occurring due to the NO_x emission decreases in all RCP scenarios and models (see Table 2 and S1). On the contrary, SRES A2 used in Wild and Palmer (2008) featured dramatic fossil fuel NO_x emission increases of 77 Tg yr^{-1}, globally, between 2000 and 2100. Regional climate changes will also play a role (predominately increasing OH through higher water vapour), and the way in which NMVOC chemistry is included in each model will certainly have large effects in the boundary layer. For example, in CMAM and HadGEM2, which do not include NMVOCs, there is less structure in tropical OH changes (Fig. S3), implying that differences in NMVOCs and their chemistry is a major contributor to regional oxidant trends in such regions.

To further examine regional changes in oxidizing capacity, we also show changes in OH in various tropospheric subdomains (divided in a way similar to Lawrence at al., 2001). Figure 7 shows large OH decreases in RCP8.5 (due to methane increases) in all regions except for the tropical and northern extratropical upper troposphere. Especially in the latter, increased stratosphere-troposphere exchange (due to a strong climate impact on the Brewer-Dobson circulation in this scenario; see Kawase et al., 2011 and Young et al., 2013) is likely a driver of positive changes, through increases of ozone available to generate OH. Also, increases in upper tropospheric humidity and lightning NO_x emissions in a warmer climate could partly explain this feature, which may be masked in the southern extratropics due to stratospheric ozone recovery leading to sizeable OH decreases. This may also yield larger OH decreases in the southern extratropical lower troposphere (-28 %) than in the Northern Hemisphere (-22 %). In RCP2.6, there is a mixture of regions with positive and negative OH changes. The lower northern extratropics show large OH decreases, presumably due to NO_x emission decreases affecting this area heavily. This effect becomes smaller with altitude (middle troposphere), presumably due to the short lifetime of NO_x.

The uncertainty in these projections is large, and in some cases it exceeds the signal of changes (for individual models, see Fig. S4). The upper troposphere tends to yield more uncertain results. In the lower troposphere, in RCP8.5, the strong impact of changing methane abundances results in a fairly strong and certain OH response. In RCP2.6, where no driver changes as dramatically, the signal-to-noise ratio is

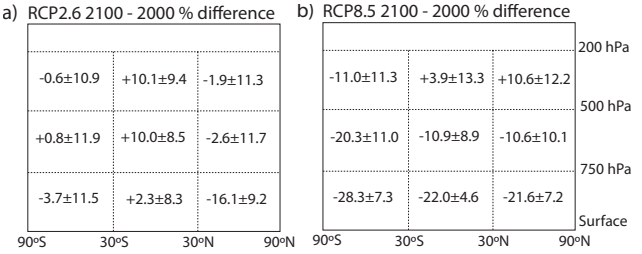

Fig. 7. Changes in regional mean OH concentration between 2100 and 2000 in various tropospheric subdomains. The range represents inter-model $\pm 1\sigma$ spread of the change.

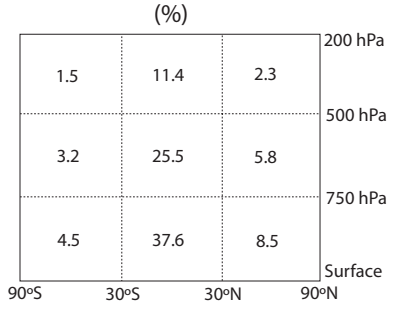

Fig. 8. The percentage of global methane that is oxidised in various subdomains of the atmosphere in present day (year 2000).

smaller. For the present day, the multi-model mean shows the largest amount of methane chemical loss in the lower tropical troposphere (Fig. 8), in excellent quantitative agreement with Lawrence et al. (2001). It is notable that in this important region, for the RCP2.6 scenario, there is little model agreement in predicted OH changes in the 21st century, with positive and negative changes being almost equally likely. Uncertainty in modelled future NMVOC emissions could be the driver of this feature.

7 Discussing diversity in model results

As mentioned earlier, an obvious conclusion of this multi-model intercomparison is the diversity in present day OH and methane lifetime. Methane tropospheric chemical lifetime in our study in year 2000 is equal to 9.8 ± 1.6 yr (see Table 1), with a spread of almost 7 yr, an almost identical value to that obtained from the ACCENT multi-model study, and with the same level of diversity (9.7 ± 1.7 yr; Shindell et al., 2006b). More recently, Fiore et al. (2009) reported a somewhat higher mean lifetime, but with a similar model spread (10.2 ± 1.7 yr). Note that in the IPCC TAR, the average tropospheric methane lifetime that was reported was 9.6 yr, though it was obtained from a smaller set of models (Prather et al., 2001).

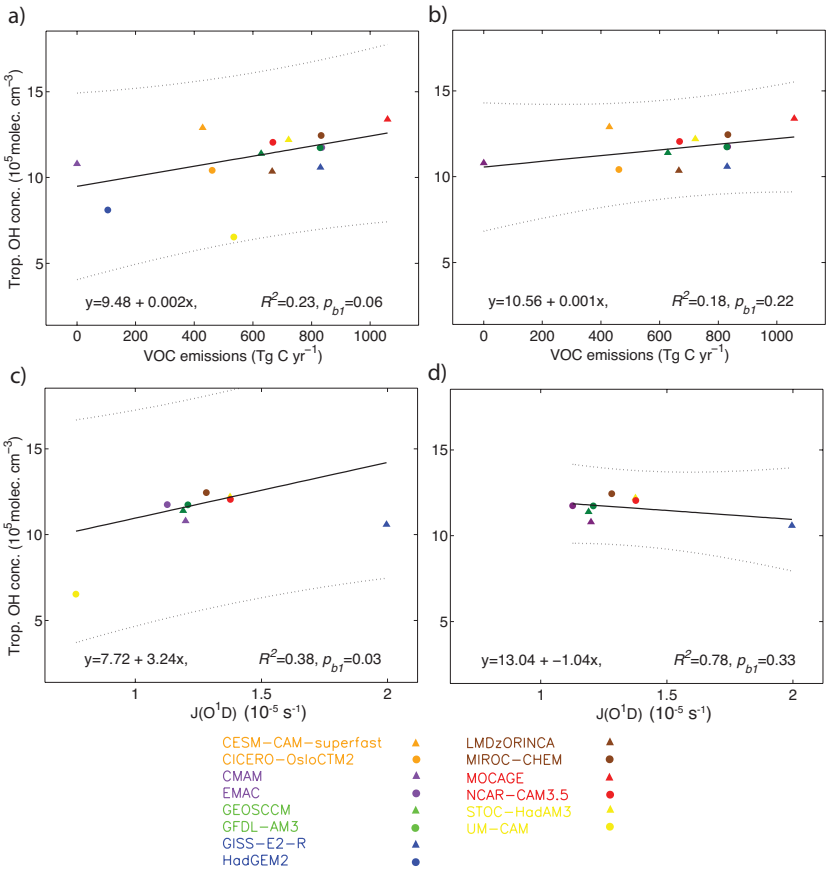

Fig. 9. Linear relationship between present day (2000) global mean tropospheric OH and **(a)** global NMVOC emissions, and **(c)** global mean $J(O^1D)$, across all models. The same relationship is shown after excluding the two models that did not have interactive photolysis, namely HadGEM2 and UM-CAM **(b, d)**. Dashed lines show the prediction intervals at a 95 % confidence level.

The models use a variety of inputs and include many interactions that are still fairly uncertain. This includes both chemical and climate variables. Here, we examine the degree to which variation across models in present day tropospheric OH and methane lifetime could be explained by the variation in emissions, tropospheric CO and ozone burden, atmospheric methane burden, stratospheric ozone column, global mean temperature, global mean specific humidity, and the global mean $J(O^1D)$. Analysis was performed over global mean values for the 2000 timeslice. Linear regression coefficients were estimated using iteratively re-weighted least squares (IRLS) regression, which is more robust than ordinary least squares (OLS) against outliers and therefore well suited to the small sample size. The full set of regression statistics for global tropospheric OH and global chemical lifetime is shown in Table S4.

Through our regression analysis we find that present day tropospheric OH spread in the models shows some association with NMVOC emissions and the $J(O^1D)$ photolysis rate. The association with $J(O^1D)$ ($p = 0.03$) is more significant than with NMVOC emissions ($p = 0.06$), though it is based on results from fewer models (only 8 models provided photolysis data). There were no apparent relationships for the remaining variables.

The positive association of global OH levels with $J(O^1D)$ is shown in Fig. 9, with the UM-CAM and GISS-E2-R falling outside of the main cluster of points. UM-CAM uses offline photolysis rates calculated in the Cambridge 2-D model, and in the past it has been shown with another model (*p*-TOMCAT) that when moving from this photolysis code to a state-of-the-art one, $J(O^1D)$ and OH levels increase significantly (Voulgarakis et al., 2009a). The outlying GISS-E2-R case can in part be explained by the fact that it has the highest CO burden among all the models, which means that the photolysis effect is masked by the consumption of OH radicals by CO. Note though that when excluding the two models that did not include interactive photolysis (HadGEM2 and UM-CAM), the relationship becomes stronger but less significant.

NMVOC emissions, which are more uncertain than NO_x and CO emissions, appear to have a positive association with OH (Fig. 9), meaning that on a global scale, their role in OH recycling is more important than their role in OH consumption (which can be large regionally). This contrasts the

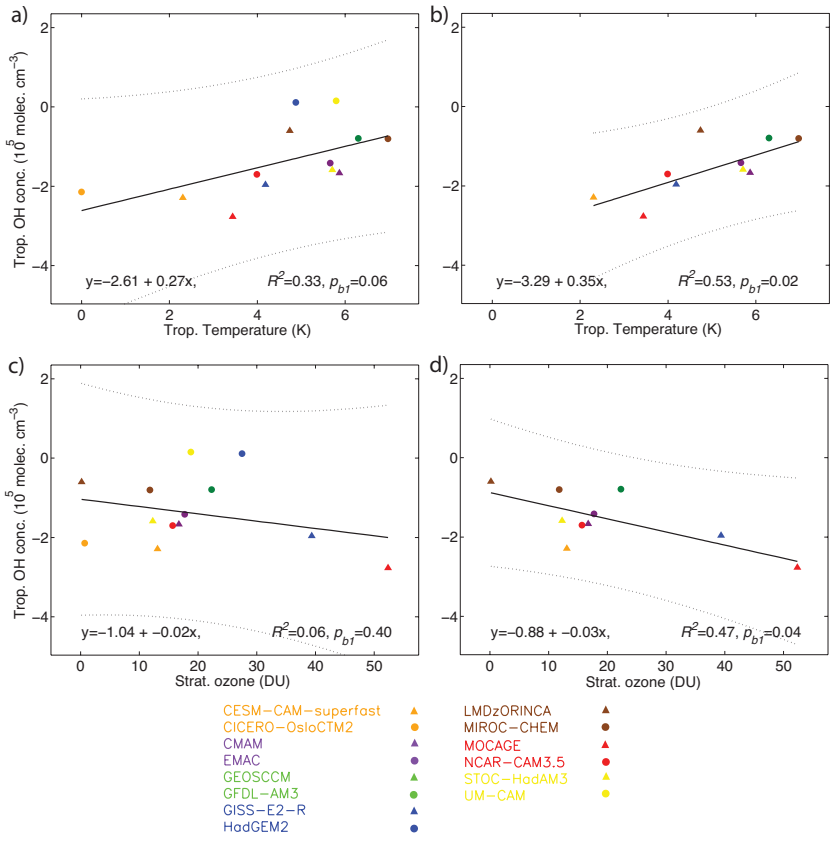

Fig. 10. Linear relationship between 2000–2100 changes in global mean tropospheric OH and 2000–2100 changes in **(a)** global mean temperature, and **(c)** global mean stratospheric ozone column, across all models. The same relationship is shown after excluding the two models that did not have interactive photolysis, namely HadGEM2 and UM-CAM, and the model that did not take into account meteorology changes between 2000 and 2100, namely CICERO-OsloCTM2 **(b, d)**. Dashed lines show the prediction intervals at a 95 % confidence level.

findings of e.g. Poisson et al. (2000) and Wang et al. (1998), who generally found that NMVOCs contribute to lower OH in the models. Generally, the reasons why NMVOC emissions are so diverse are that (a) modellers were free to choose their own biogenic sources, and (b) a wide range of NMVOC oxidation mechanisms were used in the models. The models with the lowest NMVOC emissions are CMAM (no emissions) and HadGEM2 (no vegetation emissions). HadGEM2 has the second lowest OH in ACCMIP, while CMAM is closer to the average, probably because the extra CO amount that it includes as a proxy for NMVOC oxidation is rather low (250 Tg yr^{-1}), and certainly lower than that in HadGEM2 (475 Tg yr^{-1}). UM-CAM does not have exceptionally low or high NMVOC emissions, but the fact that its photolysis is too slow makes it an outlier in terms of OH. The model with the highest abundance of OH is MOCAGE, and we speculate that this is likely explained by the fact that its NMVOC emissions are the highest of all models. Also, low stratospheric ozone columns in this model may be causing higher UV radiation resulting in greater tropospheric OH production, although it is difficult to diagnose this as photolysis rates are not available from MOCAGE (Naik et al., 2012a). When we exclude HadGEM2 and UM-CAM, the relationship becomes weaker and less significant.

To examine what drives the inter-model differences in OH in the future, we performed a similar analysis, using the difference between 2100 and 2000 values of the variables as quantities of interest. For 2100, we used data from the RCP8.5 scenario, due to the fact that it is expected to have the strongest signals. From our analysis, the strongest relationship is with changes in temperature and humidity (see Fig. 10a for temperature), two factors that strongly depend on each other. For methane lifetime (not shown) and temperature/humidity the associations are very strong ($p < 0.01$). This implies, that the differences among the models in projecting 21st century climate changes are the key driver of the differences in trends in oxidizing capacity. It is notable that the slope of the relationship that we calculate between methane lifetime and temperature change (−0.41) is not too different from the value of the climate penalty factor presented in Table 4 (0.34 ± 0.12 yr K^{-1}).

CICERO-OsloCTM2, which did not take any climate changes into account, shows one of the largest changes in OH, and CESM-CAM-superfast, which has the 2nd

highest OH change, also has the second smallest temperature/humidity changes. The rest of the models also follow this relationship, but two of them (HadGEM2 and UM-CAM) are outliers, since they are the only ones with a negative methane lifetime change, though their temperature and humidity responses are not exceptional. The unique behavior of these two models was discussed in Sect. 5.3, where we found that their methane lifetime response per unit temperature change is particularly strong, when compared to the other models.

Note that when we remove these two models from the analysis (Fig. 10b) the relationship between OH and temperature becomes even stronger and more significant. Also, in this subset of models, stratospheric ozone column becomes a significant driver of diversity, with models having stronger stratospheric ozone recovery also tending to have a stronger global OH reduction (Fig. 10c, d).

The fact that emissions, especially of NO_x and CO, and methane abundances, do not appear to be as important as NMVOC emissions and climate in driving inter-model differences in OH and methane lifetime, does not necessarily imply that emissions of such species are actually well-constrained. Rather, it means that, in terms of emissions, we performed well-constrained experiments, in order to understand what atmospheric factors can drive chemical change and diversity. This approach has been valuable, but it also has limitations, because real uncertainty in anthropogenic and natural emissions is not accounted for. Furthermore, all the RCP scenarios that are available assume that global NO_x and CO emissions from anthropogenic sources will rapidly decrease in the 21st century, which is an assumption that restricts us from examining the evolution of tropospheric composition under a less optimistic scenario for short-lived pollutants.

8 Conclusions and future work

We have analysed and discussed the evolution of OH and methane lifetime between present day and projected 2100 conditions for different RCP scenarios, as simulated by the models participating in ACCMIP. For the present day (2000), using the 14 models, we calculate a methane lifetime of 9.6 ± 1.8 yr. There is a sizeable inter-model spread in both OH and methane lifetime, which has remained almost unchanged in magnitude compared to previous multi-model studies (Shindell et al., 2006b; Fiore et al., 2009). Compared to their mean values, OH levels range by 62 % and methane lifetime ranges by 69 % across models in 2000. Based on a regression analysis, we suggest that part of this present day variability could be explained by model differences in NMVOC emissions and the treatment of photolysis. Models with high emissions of NMVOCs and high global mean photolysis rates (which are both fairly uncertain variables) tend to have higher global mean OH levels.

For the future evolution of OH and methane lifetime, mixed trends are found in the different models for each of the RCPs. In particular, diagnosing coherent changes for different regions is very challenging, due to local idiosyncrasies which are not necessarily taken into account in all models. RCP8.5 produces the largest changes in global OH and methane lifetime. Methane lifetime increases in most of the models for this scenario, driven by the large methane burden increase (doubles in 2100 compared to 2000), coupled with a smaller contribution from the effects of stratospheric ozone recovery (leading to slower photolysis and less OH in the troposphere). In the other RCP scenarios, where no such large methane perturbation is applied, the interplay between different factors leads to small changes, and a fairly stable OH and methane lifetime for these projections. Even though the model spread of results for RCP8.5 is the most coherent in terms of the sign of the change, the amount of change relative to 2000 differs among the models. We suggest that these differences mostly arise from the diversity in modelled climate changes (temperature, humidity), and possibly from differences in simulating the extent of stratospheric ozone recovery.

To elucidate the role of individual driving factors further, future experiments should focus on sensitivity simulations, changing one factor at a time in a manner similar to Wild (2007) (but focusing on OH), and performed by a range of models. The use of Gaussian process emulation, as e.g. in Lee et al. (2012), would also contribute to further understanding processes that drive the uncertainty in global oxidation simulations. Additionally, the chemical schemes need to be assessed in more detail, since their rate coefficients and reactions remains an unknown source of uncertainty. In particular, the representation of NMVOCs and their reactions under low-NO_x conditions are highly uncertain, which can lead to variations in future OH and methane lifetime projections (e.g. Archibald et al., 2011). NMVOC emissions in ACCMIP were highly variable in the different models resulting from diversity in chemical mechanisms and the biogenic source implemented in the models. Future model intercomparisons would benefit from the availability of detailed NMVOC diagnostics, such as emissions from specific sources, and OH diagnostics such as production and loss fluxes for a better understanding of the model-to-model diversity in OH. Clouds, a factor on which we did not focus in this study, could be an important driver of regional changes in OH (Voulgarakis et al., 2009b), but these effects remain to be examined systematically in a multi-model framework. Gas-aerosol interactions in future atmospheres should also be studied more thoroughly, using the knowledge on oxidants that is obtained through our analysis. The fact that global climate models are now being developed to include a range of processes which were not available until recently provides the possibility to understand atmospheric composition from a broader perspective, in which atmospheric chemistry is an integral part of the Earth system.

Appendix A

Table A1. Table of participating models and their specifications. For more information, see tables in Lamarque et al. (2013).

Model	Scenarios with simulations	Lightning NO_x^*	Stratospheric Ozone	Photolysis scheme	Methane	k_{CH_4+OH} (10^{-5} cm^3 molec^{-1} s^{-1})
CESM-CAM-superfast Rotman et al. (2004); Lamarque et al. (2011)	RCP8.5	Interactive, based on model's convection, Price et al. (1997) (PD: 4.2)	Linearised O_3 chemistry, McLinden et al. (2000)	Look-up table with correction for modelled clouds, strat. O_3 and surf. albedo, not aerosols, Madronich and Flocke (1998)	Prescribed atmospheric concentrations with spatial variation, different for each timeslice	$2.45 \times 10^{-12}\,\mathrm{e}^{-1775/T}$
CICERO-OsloCTM2, Skeie et al. (2011)	RCP2.6, RCP4.5, RCP8.5	Interactive, based on model's convection, Price et al. (1997), but scaled to 5 Tg N yr^{-1} (PD: 5.0)	Offline climatological O_3, except for the bottom 3 model strat. layers, see Skeie et al. (2011)	On-line using the Fast-J2, Wild et al. (2000); Bian and Prather (2002); accounts for modelled O_3, clouds, surf. albedo and aerosols	Prescribed surface concentrations from IPCC TAR for present day; CMIP5 future concentrations scaled to be consistent with present day levels	$2.45 \times 10^{-12}\,\mathrm{e}^{-1775/T}$
CMAM deGrandpré et al. (2000); Plummer et al. (2012)	RCP2.6, RCP4.5, RCP8.5	Interactive, based on convective updraft mass flux, modified from Allen and Pickering (2002) (PD: 3.8)	Full stratospheric chemistry	Look-up table with correction for modelled clouds, strat. O_3 and surf. albedo, not aerosols, Chang et al. (1997)	Prescribed surface concentrations following CMIP5, different in each timeslice.	$2.45 \times 10^{-12}\,\mathrm{e}^{-1775/T}$
EMAC Jöckel et al. (2006); Klinger et al (2011)	RCP4.5 RCP8.5	Interactive, Grewe et al. (2001) (PD: 5.7)	Full stratospheric chemistry	On-line, based on modelled clouds, climatological aerosol and strat. O_3, Landgraf and Crutzen (1998)	Prescribed surface concentrations using the AGAGE data for 2000, Prinn et al. (2000). CMIP5 concentration data are used to rescale AGAGE data to other years/scenarios	$1.85 \times 10^{-12} \cdot T^{2.82}\,\mathrm{e}^{-987/T}$
GEOSCCM Oman et al. (2011)	RCP6.0	Fixed emissions with a monthly climatology, based on Price et al. (1997); but scaled to 5 Tg N yr^{-1} (PD: 5.0)	Full stratospheric chemistry	Online (FastJX); accounts for clouds, strat. O_3, and albedo; uses offline aerosols from GOCART	Prescribed surface (two bottom levels) concentrations, with a prescribed latitudinal gradient, but the values are normalised so that the area-weighted mean matches the CMIP5 value for the timeslice.	$2.80 \times 10^{-14} \cdot T^{0.667}\,\mathrm{e}^{-1575/T}$
GFDL-AM3 Donner et al. (2011); Naik et al. (2012b)	RCP2.6, RCP4.5, RCP6.0 RCP8.5	Interactive, based on model's convection, Price et al. (1997), scaled so that global emissions are equal to ∼3–5 Tg N yr^{-1} for each timeslice (PD: 4.4)	Full stratospheric chemistry	Look-up table with correction for modelled clouds, strat. O_3 and surf. albedo, not aerosols, Madronich and Flocke (1998)	Prescribed surface concentrations following CMIP5, different in each timeslice.	$2.45 \times 10^{-12}\,\mathrm{e}^{-1775/T}$
GISS-E2-R Shindell et al. (2006a, 2012b)	RCP2.6, RCP4.5, RCP6.0, RCP8.5	Interactive, based on model's convection (modified from Price et al. 1997) (PD: 7.7)	Full stratospheric chemistry	Online (Fast-J2 scheme); accounts for modelled clouds, strat. O_3, aerosols, surf. albedo	Prescribed surface concentrations following CMIP5 for present day. Interactive wetland emissions for future, see Shindell et al. (2004, 2012b)	$2.45 \times 10^{-12}\,\mathrm{e}^{-1775/T}$

Table A1. Continued.

Model	Scenarios with simulations	Lightning NO_x^*	Stratospheric Ozone	Photolysis scheme	Methane	k_{CH_4+OH} (10^{-5} cm^3 molec^{-1} s^{-1})
HadGEM2 (Collins et al., 2011)	RCP2.6, RCP4.5, RCP8.5	Interactive, based on model's convection, Price and Rind (1993) (PD: 1.3)	Offline stratospheric O_3 from CMIP5 dataset	Look-up table, Law and Pyle (1993); no correction for modelled fields	Prescribed surface concentrations following CMIP5, different in each timeslice.	$2.45 \times 10^{-12}\,e^{-1775/T}$
LMDzORINCA Szopa et al. (2012)	RCP2.6, RCP4.5, RCP6.0, RCP8.5	Interactive, based on model's convection, Price et al. (1997) (PD: 6.0)	Offline stratospheric O_3 (climatology from Li and Shine (1995))	Look-up table with correction for modelled clouds, strat. O_3 and surf. albedo, not aerosols, Madronich and Flocke (1998)	Anthropogenic emissions from Lamarque et al. (2010). Fixed present day natural emissions, see Szopa et al. (2012).	$2.45 \times 10^{-12}\,e^{-1775/T}$
MIROC-CHEM Sudo et al. (2002); Watanabe et al. (2011)	RCP2.6, RCP6.0, RCP8.5	Interactive, based on model's convection, Price and Rind (1992, 1994) (PD: 9.7)	Full stratospheric chemistry	Look-up table with correction for modelled clouds, strat. O_3, surf. albedo and aerosols, Landgraf and Crutzen (1998)	Prescribed surface concentrations following CMIP5, different in each timeslice.	$2.45 \times 10^{-12}\,e^{-1775/T}$
MOCAGE Josse et al. (2004); Teyssèdre et al. (2007)	RCP2.6, RCP6.0, RCP8.5	Interactive, based on Price and Rind (1992) and Ridley et al. (2005) (PD: 5.2)	Full stratospheric chemistry	Look-up table with correction for modelled clouds, strat. O_3 and surf. albedo, not aerosols, Madronich and Flock (1998)	Prescribed surface concentrations following CMIP5, different in each timeslice.	$2.45 \times 10^{-12}\,e^{-1775/T}$
NCAR-CAM3.5 Lamarque et al. (2011, 2012);	RCP2.6, RCP4.5, RCP6.0, RCP8.5	Interactive, based on model's convection Price et al. (1997); Ridley et al. (2005), scaled to ∼3–5 Tg N yr^{-1} (PD: 4.1)	Full stratospheric chemistry	Look-up table with correction for modelled clouds, strat. O_3 and surf. albedo, not aerosols (Madronich and Flocke 1998)	Prescribed surface concentrations following CMIP5, different in each timeslice.	$2.45 \times 10^{-12}\,e^{-1775/T}$
STOC-HadAM3 Stevenson et al. (2004)	RCP2.6, RCP8.5	Interactive, based on model's convection, Price and Rind (1992); Price et al. (1997). Scaled to give ∼7 Tg N yr^{-1} (PD: 7.2)	Offline stratospheric O_3 from CMIP5 dataset	1-D, two-stream model, Hough (1988). Uses climatological O_3 above tropopause and modelled O_3 below.	Prescribed globally uniform concentrations, different for each timeslice following CMIP5 dataset	$2.45 \times 10^{-12}\,e^{-1775/T}$
UM-CAM Zeng et al. (2008, 2010)	RCP2.6, RCP4.5, RCP8.5	Interactive, based on model's convection, Price and Rind (1992, 1994) (PD: 5.2)	Offline stratospheric O_3 from CMIP5 dataset	Look-up table Law and Pyle (1993); no correction for modelled fields	Prescribed globally uniform atmospheric concentration with no spatial variation; different for each timeslice	$1.85 \times 10^{-12}\,e^{-1690/T}$

* Value in the last parenthesis represents global total present day emissions in Tg N yr^{-1}.

Supplementary material related to this article is available online at: http://www.atmos-chem-phys.net/13/2563/2013/acp-13-2563-2013-supplement.zip.

Acknowledgements. ACCMIP is organised under the auspices of the International Global Atmospheric Chemistry (IGAC) and Stratospheric Processes And their Role in Climate (SPARC) projects under the International Geosphere-Biosphere Project (IGBP) and World Climate Research Program (WCRP). The authors are grateful to the British Atmospheric Data Centre (BADC), which is part of the NERC National Centre for Atmospheric Science (NCAS), for collecting and archiving the ACCMIP data. For CESM-CAM-superfast, DB and PC were funded by the U.S. Dept. of Energy (BER), performed under the auspices of LLNL under Contract DE-AC52-07NA27344, and used the supercomputing resources of NERSC under contract No. DE11AC02-05CH11231. The CICERO-OsloCTM2 simulations were done within the projects SLAC (Short Lived Atmospheric Components) and EarthClim funded by the Norwegian Research Council. DP would like to thank the Canadian Foundation for Climate and Atmospheric Sciences for their long-running support of CMAM development. For EMAC, the work of VE and MR was funded by the DLR Earth System Model Validation (ESMVal) project and used the supercomputing resources of the German Climate Computing Center (DKRZ) and the Leibniz Supercomputing Centre (LRZ), and the work of IC was funded by the ENEA National Integrated Model to support the international negotiation on atmospheric pollution (Minni) project. The GEOSCCM work was supported by the NASA Modeling, Analysis and Prediction program, with computing resources provided by NASA's High-End Computing Program through the NASA Advanced Supercomputing Division. VN and LWH acknowledge efforts of GFDL's Global Atmospheric Model Development Team in the development of the GFDL-AM3 and Modeling Services Group for assistance with data processing. For the GISS models, support is acknowledged from the NASA MAP and ACMAP programs. For HadGEM2, WJC, GAF, and STR were supported by the Joint DECC and Defra Integrated Climate Programme (GA01101). The LMDz-OR-INCA simulations were done using computing resources provided by the CCRT/GENCI computer center of the CEA. The MOCAGE simulations were supported by Météo-France and CNRS. Supercomputing time was provided by Météo-France/DSI supercomputing centre. The MIROC-CHEM calculations were performed on the NIES supercomputer system (NEC SX-8R), and supported by the Environment Research and Technology Development Fund (S-7) of the Ministry of the Environment, Japan. The CESM project, including NCAR-CAM3.5, is supported by the National Science Foundation and the Office of 1 Science (BER) of the US Department of Energy. The National Center for Atmospheric Research is operated by the University Corporation for Atmospheric Research under sponsorship of the National Science Foundation. The STOC-HadAM3 work was supported by cross UK research council grant NE/I008063/1 and used facilities provided by the UK's national high-performance computing service, HECToR, through Computational Modelling Services (CMS), part of the NERC National Centre for Atmospheric Science (NCAS). For UM-CAM, GZ acknowledges NIWA HPCF facility and funding from New Zealand Ministry of Science and Innovation. AV thanks Chris Holmes for clarifications on the observational methane lifetime estimate.

Edited by: H. Tost

References

Allen, D. J. and Pickering, K. E.: Evaluation of lightning flash rate parameterizations for use in a global chemical transport model, J. Geophys. Res., 107, 4711, doi:10.1029/2002JD002066, 2002.

Archibald, A. T., Levine, J. G., Abraham, N. L., Cooke, M. C., Edwards, P. M., Heard, D. E., Jenkin, M. E., Karunaharan, A., Pike, R. C., Monks, P. S., Shallcross, D. E., Telford, P. J., Whalley, L. K., and Pyle, J. A.: Impacts of HOx regeneration and recycling in the oxidation of isoprene: Consequences for the composition of past, present and future atmospheres, Geophys. Res. Lett., 38, L05804, doi:10.1029/2010GL046520, 2011.

Atkinson, R., Baulch, D. L., Cox, R. A., Crowley, J. N., Hampson, R. F., Hynes, R. G., Jenkin, M. E., Rossi, M. J., and Troe, J.: Evaluated kinetic and photochemical data for atmospheric chemistry: Volume I – gas phase reactions of O_x, HO_x, NO_x and SO_x species, Atmos. Chem. Phys., 4, 1461–1738, doi:10.5194/acp-4-1461-2004, 2004.

Bian, H. and Prather, M.: Fast-J2: Accurate simulations of photolysis in global climate models, J. Atmos. Chem., 41, 281–296, 2002.

Bousquet, P., Hauglustaine, D. A., Peylin, P., Carouge, C., and Ciais, P.: Two decades of OH variability as inferred by an inversion of atmospheric transport and chemistry of methyl chloroform, Atmos. Chem. Phys., 5, 2635–2656, doi:10.5194/acp-5-2635-2005, 2005.

Bowman, K. W., Shindell, D. T., Lamarque, J.-F., Young, P. J., de la Torre, M., Worden, H., Bergmann, D., Stevenson, D., Cameron-Smith, P., Collins, W. J., Doherty, R., Dalsøren, S., Eyring, V., Faluvegi, G., Folberth, G., Ghan, S. J., Horowitz, L. W., Josse, B., Lee, Y., MacKenzie, I., Nagashima, T., Naik, V., Plummer, D., Rumbold, S., Skeie, R., Strode, S., Sudo, K., Szopa, S., Voulgarakis, A., Zeng, G. and Aghedo, A.: Observational constraints on ozone radiative forcing from the Atmospheric Chemistry Climate Model Intercomparison Project (ACCMIP), Atmos. Chem. Phys. Discuss., 12, 23603–23644, doi:10.5194/acpd-12-23603-2012, 2012.

Cagnazzo C., Manzini, E., Giorgetta, M. A., Forster, P. M. De F., and Morcrette, J. J.: Impact of an improved shortwave radiation scheme in the MAECHAM5 General Circulation Model, Atmos. Chem. Phys., 7, 2503–2515, doi:10.5194/acp-7-2503-2007, 2007.

Cionni, I., V. Eyring, J.-F. Lamarque, W. J. Randel, D. S. Stevenson, F. Wu, G. E. Bodeker, T. G. Shepherd, D. T. Shindell, and D. W. Waugh, Ozone database in support of CMIP5 simulations: results and corresponding radiative forcing. Atmos. Chem. Phys, 11, 11267–11292, doi:10.5194/acp-11-11267-2011, 2011.

Collins, W. J., Bellouin, N., Doutriaux-Boucher, M., Gedney, N., Halloran, P., Hinton, T., Hughes, J., Jones, C. D., Joshi, M., Liddicoat, S., Martin, G., O'Connor, F., Rae, J., Senior, C., Sitch, S., Totterdell, I., Wiltshire, A., and Woodward, S.: Development and evaluation of an Earth-System model – HadGEM2, Geosci. Model Dev., 4, 1051–1075, doi:10.5194/gmd-4-1051-2011, 2011.

Dalsøren, S. B. and Isaksen, I. S. A.: CTM study of changes in tropospheric hydroxyl distribution 1990–2001 and

its impact on methane, Geophys. Res. Lett., 33, L23811, doi:10.1029/2006GL027295, 2006.

Del Genio, A. D., Yao, M.-S., and Jonas, J.: Will moist convection be stronger in a warmer climate?, Geophys. Res. Lett., 34, L16703, doi:10.1029/2007GL030525, 2007.

deGrandpré, J., Beagley, S. R., Fomichev, V. I., Griffioen, E., McConnell, J. C., Medvedev, A. S., and Shepherd, T. G.: Ozone climatology using interactive chemistry: Results from the Canadian Middle Atmosphere Model, J. Geophys. Res., 105, 26475–26491, 2000.

DeMore, W. B.: Experimental and estimated rate constants for the reactions of hydroxyl radicals with several halocarbons, J. Phys. Chem., 100, 5813–5820, 1996.

Dentener, F., Peters, W., Krol, M., van Weele, M., Bergamaschi, P., and Lelieveld, J.: Interannual variability and trend of CH4 lifetime as a measure for OH changes in the 1979–1993 time period, J. Geophys. Res., 108, 4442, doi:10.1029/2002JD002916, 2003.

Donner, L. J.,Wyman, B. L., Hemler, R. S., Horowitz, L.W., Ming, Y., Zhao, M., Golaz, J.-C., Ginoux, P., Lin, S.-J., Schwarzkopf, M. D., Austin, J., Alaka, G., Cooke, W. F., Delworth, T. L., Freidenreich, S. M., Gordon, C. T., Griffies, S. M., Held, I. M., Hurlin, W. J., Klein, S. A., Knutson, T. R., Langenhorst, A. R., Lee, H.-C., Lin, Y., Magi, B. I., Malyshev, S. L., Milly, P. C. D., Naik, V., Nath, M. J., Pincus, R., Ploshay, J. J., Ramaswamy, V., Seman, C. J., Shevliakova, E., Sirutis, J. J., Stern, W. F., Stouffer, R. J., Wilson, R. J., Winton, M., Wittenberg, A. T., and Zeng, F.: The dynamical core, physical parameterizations, and basic simulation characteristics of the atmospheric component AM3 of the GFDL Global Coupled Model CM3, J. Climate, 24, 3484–3519, doi:10.1175/2011JCLI3955.1, 2011.

Eyring, V., Cionni, I., Bodeker, G. E., Charlton-Perez, A. J., Kinnison, D. E., Scinocca, J. F., Waugh, D. W., Akiyoshi, H., Bekki, S., Chipperfield, M. P., Dameris, M., Dhomse, S., Frith, S. M., Garny, H., Gettelman, A., Kubin, A., Langematz, U., Mancini, E., Marchand, M., Nakamura, T., Oman, L. D., Pawson, S., Pitari, G., Plummer, D. A., Rozanov, E., Shepherd, T. G., Shibata, K., Tian, W., Braesicke, P., Hardiman, S. C., Lamarque, J. F., Morgenstern, O., Pyle, J. A., Smale, D., and Yamashita, Y.: Multimodel assessment of stratospheric ozone return dates and ozone recovery in CCMVal-2 models, Atmos. Chem. Phys., 10, 9451–9472, doi:10.5194/acp-10-9451-2010, 2010.

Fiore, A. M., Horowitz, L. W., Dlugokencky, E. J., and West, J. J., Impact of meteorology and emissions on methane trends, 1990–2004, Geophys. Res. Lett., 33, L12809, doi:10.1029/2006GL026199, 2006.

Fiore, A. M., Dentener, F. J.,Wild, O., Cuvelier, C., Schultz, M. G., Hess, P., Textor, C., Schulz,M., Doherty, R. M., Horowitz, L.W., MacKenzie, I. A., Sanderson, M. G., Shindell, D. T., Stevenson, D. S., Szopa, S., Van Dingenen, R., Zeng, G., Atherton, C., Bergmann, D., Bey, I., Carmichael, G., Collins, W. J., Duncan, B. N., Faluvegi, G., Folberth, G., Gauss, M., Gong, S., Hauglustaine, D., Holloway, T., Isaksen, I. S. A., Jacob, D. J., Jonson, J. E., Kaminski, J. W., Keating, T. J., Lupu, A., Marmer, E., Montanaro, V., Park, R. J., Pitari, G., Pringle, K. J., Pyle, J. A., Schroeder, S., Vivanco, M. G., Wind, P., Wojcik, G., Wu, S., and Zuber, A.: Multimodel estimates of intercontinental source-receptor relationships for ozone pollution, J. Geophys. Res., 114, D04301, doi:10.1029/2008JD010816, 2009.

Forster, P., Ramaswamy, V., Artaxo, P., Berntsen, T., Betts, R., Fahey, D. W., Haywood, J., Lean, J., Lowe, D. C., Myhre, G., Nganga, J., Prinn, R., Raga, G., Schulz, M., and Van Dorland, R.: Changes in atmospheric constituents and in radiative forcing, in: Climate Change 2007: The Physical Science Basis-Contribution of Working Group I to the Fourth Assessment Report of the Intergovernmental Panel on Climate Change, edited by: Solomon, S., Qin, D., Manning, M., Chen, Z., Marquis, M., Averyt, K. B., Tignor, M., and Miller, H. L., Cambridge Univ. Press, Cambridge, UK, 2007.

Grewe, V., Brunner, D., Dameris, M., Grenfell, J. L., Hein, R., Shindell, D., and Staehelin, J.: Origin and variability of upper tropospheric nitrogen oxides and ozone at northern mid-latitudes, Atmos. Environ., 35, 3421–3433, 2001.

Gupta, M. L., Cicerone, R. J., and Elliot, S.: Perturbation to global tropospheric oxidizing capacity due to latitudinal redistribution of surface sources of NO_x, CH_4 and CO, Geophys. Res. Lett., 25, 3931–3934, 1998.

Holmes, C. D., Prather, M. J., Søvde, O. A., and Myhre, G.: Future methane, hydroxyl, and their uncertainties: key climate and emission parameters for future predictions, Atmos. Chem. Phys., 13, 285–302, doi:10.5194/acp-13-285-2013, 2013.

Hough, A. M.: The calculation of photolysis rates for use in global modelling studies, Tech. rep., UK Atomic Energy Authority, Harwell, Oxon., UK, 1988.

IPCC (Intergovernmental Panel on Climate Change): Special report on emissions scenarios: a special report of Working Group III of the Intergovernmental Panel on Climate Change, 599 pp., Cambridge University Press, Cambridge, UK, 2000.

Jacobson, M. Z. and Streets, D. G.: Influence of future anthropogenic emissions on climate, natural emissions, and air quality, Journal of Geophysical Research, 114, D08118, doi:10.1029/2008JD011476, 2009.

John, J. G., Fiore, A. M., Naik, V., Horowitz, L. W., and Dunne, J. P.: Climate versus emission drivers of methane lifetime from 1860–2100, Atmos. Chem. Phys., 12, 12021–12036, doi:10.5194/acp-12-12021-2012, 2012.

Johnson, C. E., Stevenson, D. S., Collins, W. J., and Derwent, R. G.: Role of climate feedback on methane and ozone studied with a coupled ocean-atmosphere-chemistry model, Geophys. Res. Lett., 28, 1723–1726, 2001.

Jöckel, P., Tost, H., Pozzer, A., Brühl, C., Buchholz, J., Ganzeveld, L., Hoor, P., Kerkweg, A., Lawrence, M. G., Sander, R., Steil, B., Stiller, G., Tanarhte, M., Taraborrelli, D., van Aardenne, J., and Lelieveld, J.: The atmospheric chemistry general circulation model ECHAM5/MESSy1: consistent simulation of ozone from the surface to the mesosphere, Atmos. Chem. Phys., 6, 5067–5104, doi:10.5194/acp-6-5067-2006, 2006.

Josse, B., Simon, P., and Peuch, V. H.: Radon global simulations with the multiscale chemistry and transport model MOCAGE, Tellus-B, 56, 339–356, 2004.

Kawase, H., Nagashima, T., Sudo, K., and Nozawa, T.: Future changes in tropospheric ozone under Representative Concentration Pathways (RCPs), Geophys. Res. Lett., 38, L05801, 10.1029/2010GL046402, 2011.

Klinger, Carolin, Quantitative evaluation of ozone and selected climate parameters in the chemistry-climate model EMAC, Master thesis, Ludwig Maximilian University (LMU), Munich, Ger-

many, December 2011.

Koch, D., Schmidt, G. A., and Field, C. V.: Sulfur, sea salt and radionuclide aerosols in GISS Model E, J. Geophys. Res., 111, D06206, doi:10.1029/2004JD005550, 2006.

Labrador, L. J., von Kuhlmann, R., and M. G. Lawrence, M. G.: Strong sensitivity of the global mean OH concentration and the tropospheric oxidizing efficiency to the source of NO_X from lightning, Geophys. Res. Lett., 31, L06102, doi:10.1029/2003GL019229, 2004.

Lamarque, J.-F., Bond, T. C., Eyring, V., Granier, C., Heil, A., Klimont, Z., Lee, D., Liousse, C., Mieville, A., Owen, B., Schultz, M. G., Shindell, D., Smith, S. J., Stehfest, E., Van Aardenne, J., Cooper, O. R., Kainuma, M., Mahowald, N., McConnell, J. R., Naik, V., Riahi, K., and van Vuuren, D. P.: Historical (1850–2000) gridded anthropogenic and biomass burning emissions of reactive gases and aerosols: methodology and application, Atmos. Chem. Phys., 10, 7017–7039, doi:10.5194/acp-10-7017-2010, 2010.

Lamarque, J.-F., Kyle, G. P., Meinshausen, M.. Riahi, K., Smith, S. J., van Vuuren, D. P., Conley, A., and Vitt, F.: Global and regional evolution of short-lived radiatively-active gases and aerosols in the Representative Concentration Pathways, Clim. Change, 191–212, doi:10.1007/s10584-011-0155-0, 2011.

Lamarque, J.-F, L. K. Emmons, P. G. Hess, D. E. Kinnison, S. Tilmes, F. Vitt, C. L. Heald, E. A. Holland, P. H. Lauritzen, J. Neu, J. J. Orlando, P. Rasch, G. Tyndall. CAM-chem: description and evaluation of interactive atmospheric chemistry in CESM. Geosci. Mod. Dev., 5, 369–411, doi:10.5194/gmd-5-369-2012, 2012.

Lamarque, J.-F., Shindell, D. T., Josse, B., Young, P. J., Cionni, I., Eyring, V., Bergmann, D., Cameron-Smith, P., Collins, W. J., Doherty, R., Dalsøren, S., Faluvegi, G., Folberth, G., Ghan, S. J., Horowitz, L. W., Lee, Y. H., MacKenzie, I. A., Nagashima, T., Naik, V., Plummer, D., Righi, M., Rumbold, S. T., Schulz, M., Skeie, R. B., Stevenson, D. S., Strode, S., Sudo, K., Szopa, S., Voulgarakis, A., and Zeng, G.: The Atmospheric Chemistry and Climate Model Intercomparison Project (ACCMIP): overview and description of models, simulations and climate diagnostics, Geosci. Model Dev., 6, 179–206, doi:10.5194/gmd-6-179-2013, 2013.

Landgraf, J. and Crutzen, P. J.:, An efficient method for online calculations of photolysis and heating rates, J. Atmos. Sci., 55, 863–878, 1998.

Law, K. S. and Pyle, J. A.: Modeling trace gas budgets in the troposphere 1. Ozone and odd nitrogen, J. Geophys. Res., 98, 18377–18400, 1993.

Lawrence, M. G., Jöckel, P., and von Kuhlmann, R.: What does the global mean OH concentration tell us?, Atmos. Chem. Phys., 1, 37–49, doi:10.5194/acp-1-37-2001, 2001.

Lee, L. A., Carslaw, K. S., Pringle, K. J., Mann, G. W., and Spracklen, D. V.: Emulation of a complex global aerosol model to quantify sensitivity to uncertain parameters, Atmos. Chem. Phys., 11, 12253–12273, doi:10.5194/acp-11-12253-2011, 2011.

Lelieveld, J., Crutzen, P. J., and Dentener, F. J.: Changing concentration, lifetime and climate forcing of atmospheric methane, Tellus, 50B, 128–150, 1998.

Lelieveld, J., Peters, W., Dentener, F. J., and Krol, M. C.: Stability of tropospheric hydroxyl chemistry, J. Geophys. Res., 107, 4715, doi:10.1029/2002JD002272, 2002.

Lelieveld, J., Dentener, F. J., Peters, W., and Krol, M. C.: On the role of hydroxyl radicals in the self-cleansing capacity of the troposphere, Atmos. Chem. Phys., 4, 2337–2344, doi:10.5194/acp-4-2337-2004, 2004.

Levy II, H.: Normal atmosphere: large radical and formaldehyde concentrations predicted, Science, 173, 141–143, 1971.

Li, D. and Shine, K. P.: A 4-Dimensional Ozone Climatology for UGAMP Models, UGAMP Internal Report No. 35, http://badc.nerc.ac.uk/view/badc.nerc.ac.uk__ATOM__dataent_UGAMPO3 (access date: 2 March 2013), 1995.

Logan, J. A., Prather, M. J., Wofsy, S. C., and McElroy, M. B.: Tropospheric chemistry: A global perspective, J. Geophys. Res., 86, 7210–7354, 1981.

McLinden, C. A., Olsen, S., Hannegan, B., Wild, O., Prather, M. J., and Sundet, J.: Stratospheric ozone in 3-D models: A simple chemistry and the cross-tropopause flux, J. Geophys. Res., 105, 14653–14665, 2000.

Madronich, S.: Photodissociation in the Atmosphere 1. Actinic Flux and the Effects of Ground Reflections and Clouds, J. Geophys. Res., 92, 9740–9752, 1987.

Manning, M. R., Lowe, D. C., Moss, R. C., Bodeker, G. E., and Allan, W.: Short-term variations in the oxidizing power of the atmosphere, Nature, 436, 1001–1004, doi:10.1038/nature03900, 2005.

Meehl, G. A., Stocker, T. F., Collins, W. D., Friedlingstein, P., Gaye, A. T., Gregory, J. M., Kitoh, A., Knutti, R., Murphy, J. M., Noda, A., Raper, S. C. B., Watterson, I. G., Weaver, A. J., and Zhao, Z.-C.: Global climate projections, in: Climate Change 2007: The Physical Science Basis. Contribution of Working Group I to the Fourth Assessment Report of the Intergovernmental Panel on Climate Change, edited by: Solomon, S., Qin, D., Manning, M., Chen, Z., Marquis, M., Averyt, K. B., Tignor, M., and Miller, H. L., Cambridge Univ. Press, Cambridge, UK and New York, NY, USA, 2007.

Meinshausen, M., Smith, S. J., Calvin, K., Daniel, J. S., Kainuma, M. L. T., Lamarque, J.-F., Matsumoto, K., Montzka, S., Raper, S., Riahi, K., Thomson, A., Velders, G. J. M., and van Vuuren, D. P.: The RCP Greenhouse Gas Concentrations and their Extensions from 1765 to 2300, Clim. Change, 109, 213–241, doi:10.1007/s10584-011-0156-z, 2011.

Montzka, S. A., Krol, M., Dlugokencky, E., Hall, B., Jöckel, P., and Lelieveld, J.: Small interannual variability of global atmospheric hydroxyl, Science, 331, 67–69, doi:10.1126/science.1197640, 2011.

Naik, V., Voulgarakis, A., Fiore, A. M., Horowitz, L. W., Lamarque, J.-F., Lin, M., Prather, M. J., Young, P. J., Bergmann, D., Cameron-Smith, P. J., Cionni, I., Collins, W. J., Dalsøren, S. B., Doherty, R., Eyring, V., Faluvegi, G., Folberth, G. A., Josse, B., Lee, Y. H., MacKenzie, I. A., Nagashima, T., van Noije, T. P. C., Plummer, D. A., Righi, M., Rumbold, S. T., Skeie, R., Shindell, D. T., Stevenson, D. S., Strode, S., Sudo, K., Szopa, S., and Zeng, G.: Preindustrial to present day changes in tropospheric hydroxyl radical and methane lifetime from the Atmospheric Chemistry and Climate Model Intercomparison Project (ACCMIP), Atmos. Chem. Phys. Discuss., 12, 30755–30804, doi:10.5194/acpd-12-30755-2012, 2012a.

Naik, V., Horowitz, L. W., Fiore, A. M., Ginoux, P., Mao, J., Aghedo, A., and Levy II, H.: Preindustrial to present day impact of changes in short-lived pollutant emissions on atmospheric

composition and climate forcing, resubmitted to J. Geophys. Res., 2012b.

Oman, L. D., Ziemke, J. R., Douglass, A. R., Waugh, D. W., Lang, C., Rodriguez, J. M., and Nielsen, J. E.: The response of tropical tropospheric ozone to ENSO, Geophys. Res. Lett., 38, L13706, doi:10.1029/2011GL047865, 2011.

Plummer, D. A., Scinocca, J. F., Reader, M. C., Jonsson, A. I., and Beagley, S. R.: Extension of the Canadian Middle Atmosphere Model to the troposphere, in preparation, Atmos. Chem. Phys. Discuss., 2012.

Poisson, N., Kanakidou, M., and Crutzen, P. J.: Impact of non-methane hydrocarbons on tropospheric chemistry and the oxidizing power of the global troposphere: 3-dimensional modelling results, J. Atmos. Chem., 36, 157–230, 2000.

Prather, M., Ehhalt, D., Prather, M., Dentener, F., Derwent, R., Dlugokencky, E., Holland, E., Isaksen, I., Katima, J., Kirchhoff, V., Matson, P., Midgley, P., and Wang, M.: Atmospheric chemistry and greenhouse gases, in: Climate Change 2001: The Scientific Basis. Contribution of Working Group I to the Third Assessment Report of the Intergovernmental Panel on Climate Change, edited by: Houghton, J. T., Ding, Y., Griggs, D. J., Noguer, M., van der Linden, P. J., Dai, X., Maskell, K., and Johnson, C. A., Cambridge Univ. Press, Cambridge, UK, 239–287, 2001.

Prather, M. J., Holmes, C. D., and Hsu, J.: Reactive greenhouse gas scenarios: Systematic exploration of uncertainties and the role of atmospheric chemistry, Geophys. Res. Lett., 39, L09803, doi:10.1029/2012GL051440, 2012.

Price, C. and Rind, D.: A simple lightning parameterization for calculating global lightning distributions, J. Geophys. Res., 97, 9919–9933, doi:10.1029/92JD00719, 1992.

Price, C. and Rind, D.: What determines the cloud-to-ground lightning fraction in thunderstorms?, Geophys. Res. Lett., 20, 6, 463–466, 1993.

Price, C. and Rind, D.: Modeling global lightning distributions in a general circulation model. M. Weather Rev., 122, 1930–1939, 1994.

Price, C., Penner, J., and Prather, M.: NO_x from lightning, 1, Global distribution based on lightning physics, J. Geophys. Res., 102, 5929–5941, 1997.

Prinn, R. G., Weiss, R. F., Miller, B. R., Huang, J., Alyea, F. N., Cunnold, D. M., Fraser, P. J., Hartley, D. E., and Simmonds, P. G.: Atmospheric Trends and Lifetime of CH_3CCl_3 and Global OH Concentrations, Science, 269, 187–192, 1995.

Prinn, R. G., Huang, J., Weiss, R. F., Cunnold, D. M., Fraser, P. J., Simmonds, P. G., McCulloch, A., Harth, C., Reimann, S., Salameh, P., O'Doherty, S., Wang, R. H. J.,Porter, L. W., Miller, B. R., and Krummel, P. B.: Evidence for variability of atmospheric hydroxyl radicals over the past quarter century, Geophys. Res. Lett., 32, L07809, doi:10.1029/2004GL022228, 2005.

Ridley, B. A., Pickering, K. E., and Dye, J. E.: Comments on the parameterization of lightning-produced NO in global chemistry-transport models, Atmos. Environ., 39, 6184–6187, 2005.

Rohrer, F. and Berresheim, H.: Strong correlation between levels of tropospheric hydroxyl radicals and solar ultraviolet radiation, Nature, 442, 184–187, 2006.

Rotman, D. A., Atherton, C. S., Bergmann, D. J., Cameron-Smith, P. J., Chuang, C. C., Connell, P. S., Dignon, J. E., Franz, A., Grant, K. E., Kinnison, D. E., Molenkamp, C. R., Proctor, D. D., and Tannahill, J. R.: IMPACT, the LLNL 3-D global atmospheric chemical transport model for the combined troposphere and stratosphere: Model description and analysis of ozone and other trace gases, J. Geophys. Res., 109, D04303, doi:10.1029/2002JD003155, 2004.

Shindell, D. T., Walter, B. P., and Faluvegi, G.: Impacts of climate change on methane emissions from wetlands, Geophys. Res. Lett., 31, L21202, doi:10.1029/2004GL021009, 2004.

Shindell, D. T., Faluvegi, G., Unger, N., Aguilar, E., Schmidt, G. A., Koch, D. M., Bauer, S. E., and Miller, R. L.: Simulations of preindustrial, present-day, and 2100 conditions in the NASA GISS composition and climate model G-PUCCINI, Atmos. Chem. Phys., 6, 4427–4459, doi:10.5194/acp-6-4427-2006, 2006a.

Shindell, D. T., Faluvegi, G., Stevenson, D. S., Krol, M. C., Emmons, L. K., Lamarque, J.-F., P´etron, G., Dentener, F. J., Ellingsne, K., Schultz, M. G., Wild, O., Amann, M., Atherton, C. S., Bergmann, D. J., Bey, I., Butler, T., Cofala, J., Collins, W. J., Derwent, R. G., Doherty, R. M., Drevet, J., Eskes, H. J., Fiore, A. M., Gauss, M., Hauglustaine, D. A., Horowitz, L. W., Isaksen, I. S. A., Lawrence, M. G., Montanaro, V., M¨uller, J.-F., Pitari, G., Prather, M. J., Pyle, J. A., Rast, S., Rodriguez, J. M., Sanderson,M. G., Savage, N. H., Strahan, S. E., Sudo, K., Szopa, S., Unger, N., van Noije, T. P. C., and Zeng, G.: Multimodel simulations of carbon monoxide: Comparison with observations and projected near-future changes, J. Geophys. Res., 111, D19306, doi:10.1029/2006JD007100, 2006b.

Shindell, D. T., Faluvegi, G., Koch, D. M., Schmidt, G. A., Unger, N., and Bauer, S. E.: Improved attribution of climate forcing to emissions, Science, 326, 716–718, doi:10.1126/science.1174760, 2009.

Shindell, D. T., Lamarque, J.-F., Schulz, M., Flanner, M., Jiao, C., Chin, M., Young, P., Lee, Y. H., Rotstayn, L., Milly, G., Faluvegi, G., Balkanski, Y., Collins, W. J., Conley, A. J., Dalsøren, S., Easter, R., Ghan, S., Horowitz, L., Liu, X., Myhre, G., Nagashima, T., Naik, V., Rumbold, S., Skeie, R., Sudo, K., Szopa, S., Takemura, T., Voulgarakis, A., and Yoon, J.-H.: Radiative forcing in the ACCMIP historical and future climate simulations, Atmos. Chem. Phys. Discuss., 12, 21105–21210, doi:10.5194/acpd-12-21105-2012, 2012a.

Shindell, D. T., Pechony, O., Voulgarakis, A., Faluvegi, G., Nazarenko, L., Lamarque, J.-F., Bowman, K., Milly, G., Kovari, B., Ruedy, R., and Schmidt, G.: Interactive ozone and methane chemistry in GISS-E2 historical and future climate simulations, Atmos. Chem. Phys. Discuss., 12, 23513-23602, doi:10.5194/acpd-12-23513-2012, 2012b.

Skeie, R. B., Berntsen, T. K., Myhre, G., Tanaka, K., Kvalevåg, M. M., and Hoyle, C. R.: Anthropogenic radiative forcing time series from pre-industrial times until 2010, Atmos. Chem. Phys., 11, 11827–11857, doi:10.5194/acp-11-11827-2011, 2011.

Spivakovsky, C. M., Logan, J. A., Montzka, S. A., Balkanski, Y. J., Foreman-Fowler, M., Jones, D. B. A., Horowitz, L. W., Fusco, A. C., Brenninkmeijer, C. A. M., Prather, M. J., Wofsy, S. C., and McElroy, M. B.: Three-dimensional climatological distribution of tropospheric OH: Update and evaluation, J. Geophys. Res., 105, 8931–8980, 2000.

Stevenson, D. S., Johnson, C. E., Collins, W. J., Derwent, R. G., and Edwards, J. M.: Future estimates of tropospheric ozone radiative forcing and methane turnover – The impact of climate change,

Geophys. Res. Lett., 27, 2073–2076, 2000.

Stevenson, D. S., Doherty, R. M., Sanderson, M. G., Collins, W. J., Johnson, C. E., and Derwent, R. G.: Radiative forcing from aircraft NOx emissions: Mechanisms and seasonal dependence, J. Geophys. Res., 109, D17307, doi:10.1029/2004JD004759, 2004.

Stevenson, D. S., Dentener, F. J., Schultz, M. G., Ellingsen, K., van Noije, T. P. C., Wild, O., Zeng, G., Amann, M., Atherton, C. S., Bell, N., Bergmann, D. J., Bey, I., Butler, T., Cofala, J., Collins, W. J., Derwent, R. G., Doherty, R. M., Drevet, J., Eskes, H. J., Fiore, A. M., Gauss, M., Hauglustaine, D. A., Horowitz, L. W., Isaksen, I. S. A., Krol, M. C., Lamarque, J.-F., Lawrence, M. G., Montanaro, V., Müller, J.-F., Pitari, G., Prather, M. J., Pyle, J. A., Rast, S., Rodriguez, J. M., Sanderson, M. G., Savage, N. H., Shindell, D. T., Strahan, S. E., Sudo, K., and Szopa, S.: Multi-model ensemble simulations of present day andnear-future tropospheric ozone. J. Geophys. Res., 111, D08301, doi:10.1029/2005JD006338, 2006.

Stevenson, D. S., Young, P. J., Naik, V., Lamarque, J.-F., Shindell, D. T., Voulgarakis, A., Skeie, R. B., Dalsøren, S. B., Myhre, G., Berntsen, T. K., Folberth, G. A., Rumbold, S. T., Collins, W. J., MacKenzie, I. A., Doherty, R. M., Zeng, G., van Noije, T. P. C., Strunk, A., Bergmann, D., Cameron-Smith, P., Plummer, D. A., Strode, S. A., Horowitz, L., Lee, Y. H., Szopa, S., Sudo, K., Nagashima, T., Josse, B., Cionni, I., Righi, M., Eyring, V., Conley, A., Bowman, K. W., and Wild, O.: Tropospheric ozone changes, radiative forcing and attribution to emissions in the Atmospheric Chemistry and Climate Model Inter-comparison Project (ACCMIP), Atmos. Chem. Phys. Discuss., 12, 26047–26097, doi:10.5194/acpd-12-26047-2012, 2012.

Sudo, K., Takahashi, M., Kurokawa, J., and Akimoto, H.: CHASER: a global chemical model of the troposphere – 1. model description, J. Geophys. Res., 107, D174339, doi:10.1029/2001JD001113, 2000.

Szopa S., Balkanski, Y., Schulz, M., Bekki, S., Cugnet, D., Fortems-Cheiney, A., Turquety, S., Cozic, A., Déandreis, C., Hauglustaine, D., Idelkadi, A., Lathiére, J., Lefevre, F., Marchand, M., Vuolo, R., Yan, N., and Dufresne, J.-L.: Aerosol and Ozone changes as forcing for Climate Evolution between 1850 and 2100, Clim. Dynam., doi:10.1007/s00382-012-1408-y, 2012.

Thompson, A. M.: The oxidizing capacity of the Earth's atmosphere: Probable past and future changes, Science, 256, 1157–1168, 1992.

Teyssèdre, H., Michou, M., Clark, H. L., Josse, B., Karcher, F., Olivié, D., Peuch, V.-H., Saint-Martin, D., Cariolle, D., Attié, J.-L., Nédélec, P., Ricaud, P., Thouret, V., van der A, R. J., Volz-Thomas, A., and Chéroux, F.: A new tropospheric and stratospheric Chemistry and Transport Model MOCAGE-Climat for multi-year studies: evaluation of the present day climatology and sensitivity to surface processes, Atmos. Chem. Phys., 7, 5815–5860, doi:10.5194/acp-7-5815-2007, 2007.

van Vuuren, D. P., Edmonds, J., Kainuma, M., Riahi, K., Thomson, A., Hibbard, K., Hurtt, G. C., Kram, T., Krey, V., Lamarque, J.-F., Matsui, T., Meinshausen, M., Nakicenovic, N., Smith, S. J., and Rose, S. K.: The Representative Concentration Pathways: An overview, Clim. Change, 109, 5–31, doi:10.1007/s10584-011-0148-z, 2011.

Voulgarakis, A., Savage, N. H., Wild, O., Carver, G. D., Clemitshaw, K. C., and Pyle, J. A.: Upgrading photolysis in the p-TOMCAT CTM: model evaluation and assessment of the role of clouds, Geosci. Model Dev., 2, 59–72, doi:10.5194/gmd-2-59-2009, 2009a.

Voulgarakis, A., Wild, O., Savage, N. H., Carver, G. D., and Pyle, J. A.: Clouds, photolysis and regional tropospheric ozone budgets, Atmos. Chem. Phys., 9, 8235–8246, doi:10.5194/acp-9-8235-2009, 2009b.

Voulgarakis, A., Yang, X., and Pyle, J. A.: How different would tropospheric oxidation be over an ice-free Arctic? Geophys. Res. Lett., 36, L23807, doi:10.1029/2009GL040541, 2009c.

Wang, Y. H. and Jacob, D. J.: Anthropogenic forcing on tropospheric ozone and OH since preindustrial times, J. Geophys. Res., 103, 31123–31135, 1998.

Watanabe, S., Hajima, T., Sudo, K., Nagashima, T., Takemura, T., Okajima, H., Nozawa, T., Kawase, H., Abe, M., Yokohata, T., Ise, T., Sato, H., Kato, E., Takata, K., Emori, S., and Kawamiya, M.: MIROC-ESM 2010: model description and basic results of CMIP5-20c3m experiments, Geosci. Model Dev., 4, 845–872, doi:10.5194/gmd-4-845-2011, 2011.

Wild, O.: Modelling the global tropospheric ozone budget: exploring the variability in current models, Atmos. Chem. Phys., 7, 2643-2660, doi:10.5194/acp-7-2643-2007, 2007.

Wild, O. and Palmer, P. I.: How sensitive is tropospheric oxidation to anthropogenic emissions?, Geophys. Res. Lett., 35, L22802, doi:10.1029/2008GL035718, 2008.

Wild, O. and Prather, M. J.:, Excitation of the primary tropospheric chemical mode in a global three-dimensional model, J. Geophys. Res., 105, 24647–24660, doi:10.1029/2000JD900399, 2000.

Wu, S., Mickley, L. J., Leibensperger, E. M., Jacob, D. J., Rind, D., and Streets, D. G., Effects of 2000–2050 global change on ozone air quality in the United States, J. Geophys. Res., 113, D06302, doi:10.1029/2007JD008917, 2008.

Young, P. J., Archibald, A. T., Bowman, K. W., Lamarque, J.-F., Naik, V., Stevenson, D. S., Tilmes, S., Voulgarakis, A., Wild, O., Bergmann, D., Cameron-Smith, P., Cionni, I., Collins, W. J., Dalsøren, S. B., Doherty, R. M., Eyring, V., Faluvegi, G., Horowitz, L. W., Josse, B., Lee, Y. H., MacKenzie, I. A., Nagashima, T., Plummer, D. A., Righi, M., Rumbold, S. T., Skeie, R. B., Shindell, D. T., Strode, S. A., Sudo, K., Szopa, S., and Zeng, G.: Pre-industrial to end 21st century projections of tropospheric ozone from the Atmospheric Chemistry and Climate Model Intercomparison Project (ACCMIP), Atmos. Chem. Phys., 13, 2063–2090, doi:10.5194/acp-13-2063-2013, 2013.

Zeng, G., Pyle, J. A., and Young, P. J.: Impact of climate change on tropospheric ozone and its global budgets, Atmos. Chem. Phys., 8, 369–387, doi:10.5194/acp-8-369-2008, 2008.

Zeng, G., Morgenstern, O., Braesicke, P., and Pyle, J. A.: Impact of stratospheric ozone recovery on tropospheric ozone and its budget. Geophys. Res. Lett., 37, L09805, doi:10.1029/2010GL042812, 2010.